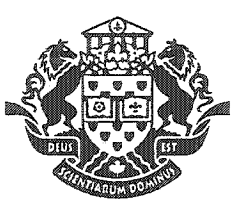

Université d'Ottawa · University of Ottawa

Université d'Ottawa · University of Ottawa

FACULTÉ DES ÉTUDES SUPÉRIEURES ET POSTDOCTORALES

FACULTY OF GRADUATE AND POSTDOCTORAL STUDIES

WAYNE, Walter

AUTEUR DE LA THÈSE - AUTHOR OF THESIS

M.A.Sc. (Electrical Engineering)

GRADE - DEGREE

School of Information Technology and Engineering

FACULTÉ, ÉCOLE, DÉPARTEMENT - FACULTY, SCHOOL, DEPARTMENT

TITRE DE LA THÈSE - TITLE OF THE THESIS

An Automated Matching Network Incorporating a Six-Port Reflectometer

P. Berini

DIRECTEUR DE LA THÈSE - THESIS SUPERVISOR

L. Roy

CO-DIRECTEUR DE LA THÈSE - THESIS CO-SUPERVISOR

EXAMINATEURS DE LA THÈSE - THESIS EXAMINERS

C. Plett

M. Yagoub

J.-M. De Koninck, Ph.D.

LE DOYEN DE LA FACULTÉ DES ÉTUDES SUPÉRIEURES ET POSTDOCTORALES

SIGNATURE

DEAN OF THE FACULTY OF GRADUATE AND POSTDOCTORAL STUDIES

An Automated Matching Network

Incorporating a Six-Port Reflectometer

By

Walter Wayne, B.A.Sc.

A thesis submitted to the
School of Graduate Studies and Research
in partial fulfillment of the requirements for the degree of

Masters of Applied Science
In Electrical Engineering

Ottawa-Carleton Institute for Electrical and Computer Engineering
School of Information Technology and Engineering
Faculty of Engineering
University of Ottawa

© Walter Wayne, Ottawa, Canada, 2003

National Library
of Canada

Acquisitions and
Bibliographic Services

395 Wellington Street
Ottawa ON K1A 0N4
Canada

Bibliothèque nationale
du Canada

Acquisisitons et
services bibliographiques

395, rue Wellington
Ottawa ON K1A 0N4
Canada

Your file Votre référence
ISBN: 0-612-90357-5
Our file Notre référence
ISBN: 0-612-90357-5

The author has granted a non-exclusive licence allowing the National Library of Canada to reproduce, loan, distribute or sell copies of this thesis in microform, paper or electronic formats.

L'auteur a accordé une licence non exclusive permettant à la Bibliothèque nationale du Canada de reproduire, prêter, distribuer ou vendre des copies de cette thèse sous la forme de microfiche/film, de reproduction sur papier ou sur format électronique.

The author retains ownership of the copyright in this thesis. Neither the thesis nor substantial extracts from it may be printed or otherwise reproduced without the author's permission.

L'auteur conserve la propriété du droit d'auteur qui protège cette thèse. Ni la thèse ni des extraits substantiels de celle-ci ne doivent être imprimés ou aturement reproduits sans son autorisation.

In compliance with the Canadian Privacy Act some supporting forms may have been removed from this dissertation.

Conformément à la loi canadienne sur la protection de la vie privée, quelques formulaires secondaires ont été enlevés de ce manuscrit.

While these forms may be included in the document page count, their removal does not represent any loss of content from the dissertation.

Bien que ces formulaires aient inclus dans la pagination, il n'y aura aucun contenu manquant.

Canada

Abstract

In this thesis an automated matching network is investigated as a means to reduce mismatch loss in circuits whose impedance characteristics vary during operation. The automated matching network incorporates a six-port network to measure impedance and a tunable circuit is implemented using varactor diodes to provide continuously variable impedances. A novel implementation for two-port measurements using a single reflectometer is presented.

The thesis concentrates on variable gain amplifier applications as these are common in wireless applications and matching is rarely maintained over the operating range of the device. A six-port reflectometer is implemented using off-the-shelf components. The tunable network is implemented using a miniature hybrid microwave integrated circuit (MHMIC) process with varactor diodes used as variable capacitances. Gain matching of a transistor amplifier is tested under various device biases.

The project establishes design guidelines for a tunable matching network using continuously variable impedances. The feasibility of the automated matching network concept is also proven. Based on the results, several proposals are made for future work using automated matching networks.

Table of Contents

List of Figures

Glossary of Terms

AMN	Automated Matching Network
BJT	Bipolar Junction Transistor
CPU	Central Processing Unit
DUT	Device Under Test
FET	Field Effect Transistor
MEMS	Micro-Electro-Mechanical Systems
MHMIC	Miniature Hybird Microwave Integrated Circuit
PA	Power Amplifier
PAE	Power Added Efficiency
SP4T	Single Pole Four Throw switch
TRL	Thru- Reflect Line calibration
VCMN	Voltage Controlled Matching Network
VGA	Variable Gain Amplifier
VGPA	Variable Gain Power Amplifier

Chapter 1: Introduction

This thesis involves the design and implementation of an automated matching network. This chapter discusses the incentive to create such a circuit, the objectives of the thesis and gives and outline of the chapters to follow.

1.1 Motivation

The popularity of wireless communication is driving the development of variable gain power amplifiers. Mobile hand-sets and base-stations must be capable of delivering high power when distance or a noisy environment requires it, and they must also be capable of reduced output when signal fidelity can be maintained at lower power transmission levels. Lowering the power prevents overloading of the receiver and reduces the probability of interfering with adjacent channels. Minimizing output power in a handset also increases battery life. High current consumption requires large batteries and thus increases the size of the product.

Several wireless applications are currently seeking a place in both personal and business uses. Bluetooth is targeting low-cost low-bandwidth (1 Mb/s) market and several IEEE 802.11 (11 Mb/s) protocols are seeking to replace cables as the link of choice in LAN applications. Bluetooth is targeting personal electronics, in which data can be transferred to and from a personal computer without requiring a connection to be made, and in other low bit-rate applications such as substituting for parallel- or serial-port cables in connecting to peripherals. Both these protocols require the capability for variable output from the transmitter.

New cellular phone protocols are expanding into higher frequency bands in order to use the bandwidth available. The variable output requirement and the higher frequency carriers used often put greater demands on the transmitter. Since higher frequency applications tend to use smaller antennas, and the high bit-rate protocols require high linearity (due to use of variable envelope modulation), producing an efficient final stage power amplifier becomes of greater importance.

Variable gain power amplifiers (VGPA) are also becoming more desirable in the realm of wireline technologies. For instance, in many cable specifications a large dynamic range is required. Since most cable connections were installed with television broadcast in mind, cables connections vary widely in loss. Having a variable gain function on a cable amplifier allows efficient use of the connections regardless of loss. In some cases, cable applications require a delineation box at the client site. While it may initially appear odd that companies would be concerned with an additional 10 or 20 mA of current consumption at the delineation box, when considering the size of the market it becomes obvious that any company with a significant share of the market would benefit on small power savings on a per link basis. Several milliAmps across several thousand circuits can result in a large difference in total power consumption and operating costs.

Most VPGAs suffer from poor efficiency under low gain conditions [4-5, as well as data sheets from component manufacturers such as RFMD or SiGe Semiconductor, Inc.]. A variable impedance tuning could be used to create an automated matching network that would reduce inefficiency resulting from the mismatch introduced. Variable impedance

tuners have already been researched [6]. However, they are typical used for post-production tuning or automated load-pull and noise measurements. This thesis will focus on the use for automated matching during normal operation.

Many wireless applications may also exhibit a variance in antenna impedance depending on the environment the antenna is currently working in [1]. An automated matching network would ensure a consistent transfer of power to the antenna under a variety of conditions.

1.2 Objectives

The first objective of the thesis is to implement and test several aspects of a six-port reflectometer suitable for use in the proposed automated matching network scheme.

The second objective is the design and implementation of a voltage controlled matching network at a frequency of approximately 10 GHz using an MHMIC process.

The third objective is to combine the six-port reflectometer and the voltage controlled matching network to measure the 2-port s-parameters of a device required in order to calculate gain matching.

The final objective involves using the measurements to implement power gain matching over several device biases.

1.3 Thesis Organization

Chapter 2 gives background information required for the thesis. It discusses gain and power matching considerations and gives several gain definitions. Current VGPA solutions are discussed. The benefits of using an automated matching network are listed. The reasons behind the choice of architecture are given.

Chapter 3 looks at six-port metrology, beginning with a look at four-port reflectometers, then expands to six-port reflectometer design and calibration. It also extends the theory to two-port circuit measurement with dual reflectometers and a novel method using a single reflectometer and a calibrated variable load. A six-port reflectometer is built and tested.

Chapter 4 covers design and implementation of a voltage-controlled matching network. Modeling, layout and technology issues are discussed and the final implementation is measured and compared to expected values. Sources of error are discussed.

Chapter 5 involves the implementation of an automated matching network for power gain matching.

Chapter 6 gives an overall conclusion to the thesis and discusses future research possibilities including improved architectures for automated matching network implementation.

Chapter 2: Matching Issues and Project Overview

This chapter gives the background information that is a foundation for the rest of the thesis. It looks at efficiency considerations, matching theory, current power amplifier (PA) solutions and the benefits of using an automated matching network (AMN). Several gain definitions are given in order to clarify language in later chapters. It then looks at two possible architectures for an AMN and describes the reasons behind choosing the design implemented in this thesis.

2.1 Efficiency Considerations

Looking at a general architecture for the front-end of a communication link, as shown in Figure 2.1, there are many components which determine the efficiency of the overall system. However, current required by most stages is dependant on the output RF power required of it, and since signal levels remain relatively low until just prior to the antenna the efficiency is primarily determined by the last few stages of the transmit chain.

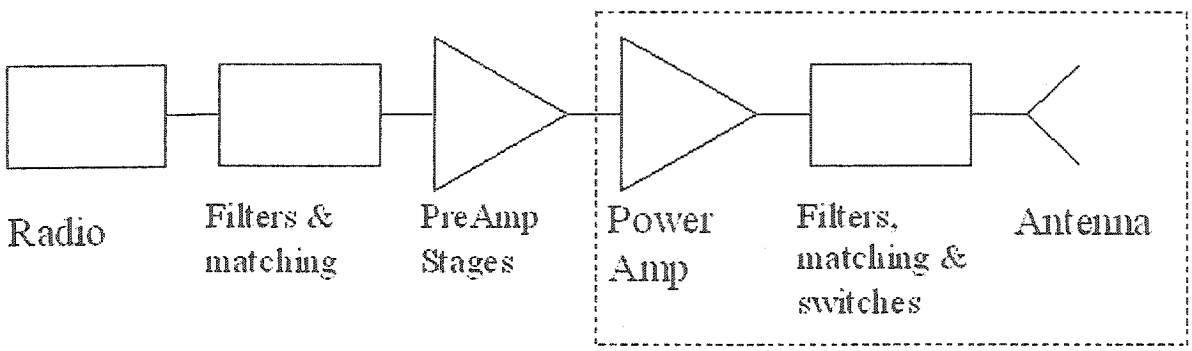

Figure 2.1:Simplified radio transmitter circuit. The final stages which dominate efficiency calculations are high lighted.

In many cases we can approximate the efficiency by looking at power amplifier efficiency, switching and filtering loss between amplifier and antenna, and the antenna efficiency. The current consumption of preceding stages is usually much below that of the PA. Inefficiencies are caused by three principle factors: mismatch loss, resistive loss, and load-line matching of the power amplifier. Resistive loss will not be discussed in detail in this section; however, for most practical microwave circuit realizations this loss is already minimized.

2.1.1 Linear Matching

A good match on a single port component such as an antenna affects the efficiency of the overall circuit. In the case of the antenna, if only 80% of the power available to it is radiated, the preceding circuit must be able to produce that much more power than if the antenna were perfectly matched. Since current consumption of a given architecture goes up proportionally with the power required, it is desirable to minimize the mismatch loss in all stages following the power amplifier. For a circuit with a reflection coefficient Γ, the mismatch loss is described by:

$$Mismatch\ Loss = 1 - |\Gamma|^2 \qquad (2.1)$$

In the case of two port circuits, simultaneous matching of both ports ensures best over all gain (or minimized loss in the case of passive circuits and switches). For a power transistor the load impedance is determined by the power output requirement, while input is typically matched to minimize mismatch [3]. Simultaneous matching of circuits for high gain (and in

the case of the PA input matching for best gain) reduces the required output power of preceding circuits (and their DC supply requirement) and thus increases overall efficiency of the circuit.

2.1.2 Effects of Linear Mismatch on Non-Linear PA Circuits

In PAs it is worth noting that the input compression point of the final transistor, $P_{in,1dB}$ can be described by:

$$P_{in,1dB} = P_{out,1dB} - G_{lin} + 1 \qquad (2.2)$$

Where $P_{out,\ 1dB}$ is output compression point and G_{lin} is the linear gain. In order for the overall system to maintain linearity, the stage preceding the power transistor must be backed off from its own $P_{out,\ 1dB}$ significantly so that it does not contribute additional non-linearity. If the final stage has low gain then, with the required back-off the preceding stage, that preceding stage will require proportionally more bias current. If the second last stage is operating a significant current compared to the final stage, efficiency drops significantly. A good input match on the final stage increases gain and ensures the stages prior to it in the RF chain need not contribute a significant amount of current.

2.1.3 Load-line matching

In the case of power amplifiers, the output match is optimized for linearity as well as gain specification. While there are many methods for linearizing PAs, load-line optimization of a

near A class device is the most frequently used [3]. Some amplifier topologies, such as S-class switching amplifiers work on different principles, these are rarely employed in the microwave regime due to their design complexity and the tendency for industries to stick to tried and true methodologies. For this reason this explanation will focus on load line matching as found in the most common amplifier schemes.

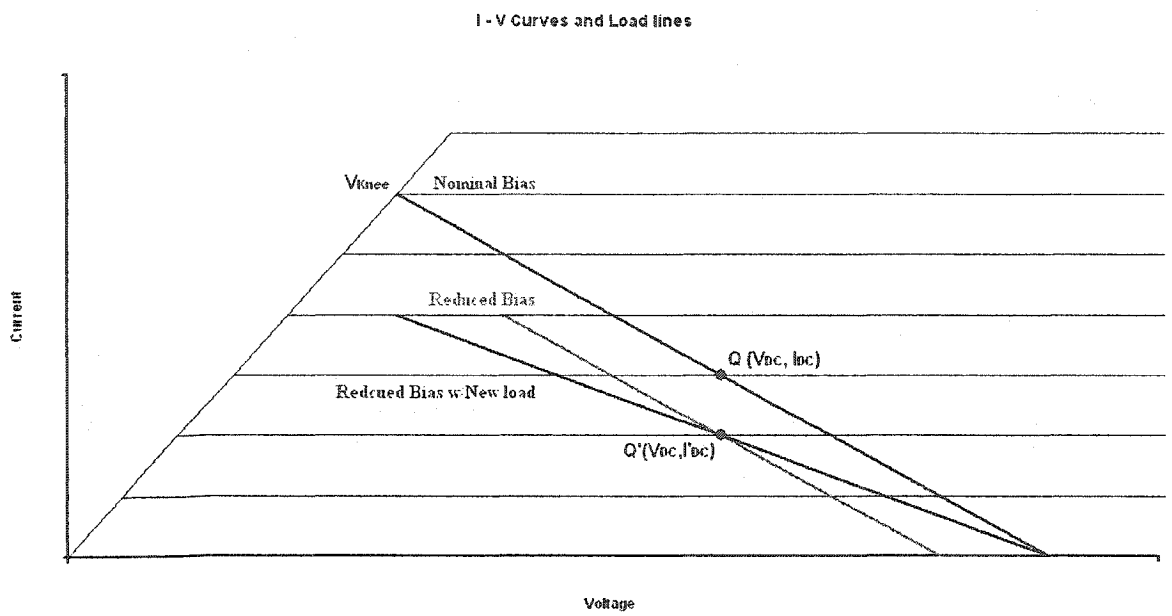

Figure 2.2: Idealized I-V curves with load-lines. Nominal bias is an optimized load-line around the Q-point (V_{DC},I_{DC}). Reduced bias depicts the linear load-line of the same device at two-thirds bias (V_{DC}, I_{DC}'). The final line shows reduced bias, but with re-optimized impedance on the load.

Looking at the active region of a BJT transistor, we can see the optimum load-line for maximizing linear power out for a given bias point, Q. Figure 2.2 shows the load-line for an idealized BJT, where the I-V curves are assumed to be almost ideal within the active region, with the exception of the introduction of a knee-voltage as the transistor moves towards saturation. Breakdown voltage is not shown as it is often of less concern with respect to the RF load-line, since the RF impedance on the base of a PA is often very low, excess charge in

the base is drained efficiently. This reduces the avalanche affect and results in a breakdown voltage for the RF swing that is generally much higher than the nominal DC breakdown given in the specification.

Calculating the power added efficiency, *PAE*, in the idealized case we compare the RF power added to the DC power supplied. The RF power output is half the product of the peak voltage swing, V_{out}, and the peak current swing, I_{out}. If the PA has significant gain the power input is much less the power output and can be neglected in the equation.

$$PAE = \frac{P_{out} - P_{in}}{P_{DC}}$$
$$PAE \approx \frac{0.5 V_{out} I_{out}^{*}}{V_{DC} I_{DC}}, \; assu\min g \; Pin \approx 0 \qquad (2.3a)$$

From the idealized graph above, at compression the peak RF current swing, I_{out}, is equal to I_{DC}. The peak RF voltage swing, V_{out} is the equal to the difference between V_{DC} and the V_{knee} on the optimum load line. Putting these in the above equation yields.

$$PAE \approx \frac{0.5(V_{DC} - V_{Knee}) I_{DC}}{V_{DC} I_{DC}}$$
$$PAE \approx \frac{V_{DC} - V_{Knee}}{2V_{DC}} \qquad (2.3b)$$

When less power is required the bias in the final PA is often lowered in order to conserve current, but the load impedance presented remains the same. Since the load does not change the slope of the load-line (- 1/Load Resistance) also remains constant. The Reduced Bias line in Figure 2.2 corresponds to reduced current bias with a constant load resistance. In this case, the DC power consumption is cut by factor of 2, while both the maximum linear voltage and current swing are also cut by a factor of 2. This means while DC power in is halved, the RF power out at the compression point is quartered. This leads to an efficiency in lower bias condition that is half that of the nominal. Also note maximum linear output power is cut by 6 dB.

To maintain efficiency the low-bias state requires an output resistance that is twice that of the nominal high bias, as shown by the Reduced Bias with New Load line in Figure 2.2. Such a system not only maintains efficiency, but linear power out is cut by only 3 dB. This has another beneficial effect in terms of linearity. Often gain drops much slower than $P_{out,\,1dB}$ as a function of reduced bias current [3]. Since gain drops slowly, this drop in $P_{out,\,1dB}$ results in a similar drop in $P_{in,\,1dB}$ (see equation 2.2), which requires the circuit to compensate for the drop in compression point by dropping the input power. By reducing the change in compression point, less variability in the driving circuit is required to compensate for the $P_{in,1dB}$. In many applications the output impedance of the device is much lower than the optimum load line. Thus increasing the output impedance as bias is lowered will result in a reduced gain as well, which will compensate for the reduction in $P_{out,1dB}$. This will further reduce the need for variable output on the front end. This is desirable as removing variable

input requirements will simplify the design of the preceding radio, and add value to the final stage design as a result.

2.2 Gain Definitions

In order to clarify some of the experiments in later chapters, gain definitions must be clarified. Also stability equations and a discussion of the information required in order to calculate matching and gain of a device are given. Figure 2.3 shows an amplifier with source and load impedances and power definitions.

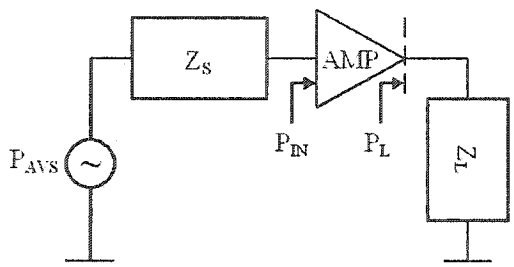

Figure 2.3: Amplifier and power definitions

The transducer gain, G_T is defined as the ratio of the power delivered to the load to the power available from the source [2]. It is a function of both input and output matching of the DUT.

$$G_T = \frac{1-|\Gamma_S|^2}{|1-\Gamma_{IN}\Gamma_S|^2}|s_{21}|^2\frac{1-|\Gamma_L|^2}{|1-s_{22}\Gamma_L|^2} \qquad (2.4)$$

The Available Gain, G_A is defined as the ratio of the power available from the DUT to the power available from the source. It is a function of the input match. Because G_A is defined

in terms of power available from the DUT and not power delivered to the load, it is independent of the output match. In the case where the output match is optimized, G_A is equal to G_T.

$$G_A = \frac{1-|\Gamma_S|^2}{|1-s_{11}\Gamma_S|^2}|s_{21}|^2 \frac{1}{1-|\Gamma_{OUT}|^2} \tag{2.5}$$

The Power Gain, G_P is defined as the ratio of the power delivered to the load to the power delivered to the DUT. It is a function of the output match. Because G_P is defined in terms of power delivered to the DUT and not power available from the source, it is independent of the input match. In the case where the input match is optimized, G_P is equal to G_T.

$$G_P = \frac{1}{1-|\Gamma_{IN}|^2}|s_{21}|^2 \frac{1-|\Gamma_L|}{|1-s_{22}\Gamma_L|^2} \tag{2.6}$$

In each of these cases we would also like to know the maximum available value for the gains. Since maximum gain is achieved under simultaneous match, and under optimum matching conditions both G_A and G_P are equal to G_T one need only look at G_{Tmax} in order to define the maximum gain for each definition. Since G_{Tmax} is dependent on stability parameters we must also define these.

The equations for gain, stability and matching are shown below for reference.

Stability conditions: $$K > 1, |\Delta| < 1, |s_{11}| < 1, |s_{22}| < 1 \quad (2.7)$$

Where:
$$K = \frac{1 - |s_{11}|^2 - |s_{22}|^2 + |\Delta|^2}{2 s_{21} s_{12}}$$
$$\Delta = s_{11} s_{22} - s_{21} s_{12}$$

Gain:
$$G_{MSG} = \frac{|s_{21}|}{|s_{12}|}, K < 1$$
$$G_{MAG} = \frac{|s_{21}|}{|s_{12}|}(K - \sqrt{K^2 - 1}), K > 1 \quad (2.8)$$

Optimum Match: $$\Gamma_{MS} = \frac{B_1 \pm \sqrt{B_1^2 - 4|C_1|^2}}{2C_1} \qquad \Gamma_{ML} = \frac{B_2 \pm \sqrt{B_2^2 - 4|C_2|^2}}{2C_2} \quad (2.9)$$

Where:
$$B_1 = 1 + |s_{11}|^2 - |s_{22}|^2 - |\Delta|^2 \qquad B_2 = 1 - |s_{11}|^2 + |s_{22}|^2 - |\Delta|^2$$
$$C_1 = s_{11} - \Delta s_{22}^* \qquad C_2 = s_{22} - \Delta s_{11}^*$$

The equation for G_T, G_A, and G_P can be solved for matching purposes knowing s_{11}, s_{22}, $|s_{21}|$ and the product $s_{21}s_{12}$. Stability criterion and optimum matches can also be determined using those s-parameters. The maximum achievable gain and maximum stable gain also require knowledge of $|s_{12}|$.

We can also defined normalized gains, by dividing the above gains by $|s_{21}|^2$. This gives us the following gain definitions.

$$g_{T\max} = \frac{1}{|s_{21}s_{12}|}, K < 1$$
$$g_{T\max} = \frac{1}{|s_{21}s_{12}|}(K - \sqrt{K^2 - 1}), K > 1 \qquad (2.10)$$

$$g_A = \frac{1-|\Gamma_S|^2}{|1-s_{11}\Gamma_S|^2}\frac{1}{1-|\Gamma_{OUT}|^2}$$
$$g_P = \frac{1}{1-|\Gamma_{IN}|^2}\frac{1-|\Gamma_L|}{|1-s_{22}\Gamma_L|^2} \qquad (2.11)$$

These gains can be calculated without knowledge of $|s_{21}|$ and $|s_{12}|$. Stability and matching performed with these normalized gains requires only knowledge of the s_{11}, s_{22}, and the product $s_{21}s_{12}$. In Chapter 3 it will be shown that this can be used to simplify the overall circuit for the automated matching network.

2.3 Current Solutions

A number of ways to achieve variable output amplifiers have been used in various applications [4-5,8-15]. A variable output radio feeding a fixed power amplifier is one simple solution that has been used. However, this is inefficient as the power amplifier

continues to consume high current even under low power conditions. This method is mainly used in first pass designs and will not be discussed further.

Variable attenuation schemes in which an attenuator proceeds the last stage can be used, however this has incredibly poor efficiency at low gains and, assuming that the isolation of the device is not high, the optimum output match changes. The final power stage rarely has high isolation, as a wide device is required to handle the output power. The additional width results in an increased capacitance between input and output thus lowering the isolation at high frequencies. The result is increased mismatch loss as attenuation changes.

Switched devices [8-10], in which different transistors are switched in for different gain states can achieve the variable power required. This includes switched gate devices in which parts of a FET are turned on or off to effectively change the width of the device and results in a variable gain and power out. Note that these schemes alter the output impedance of the device, and the current through the last device changes. Thus both the optimum gain matches and the optimum load line for power are then changed (optimum impedances are increased as thinner devices are switched in). This cuts into the efficiency of the device as the gain is dropped.

Variable bias devices reduce the current to the transistors, when in low power states. In most devices the compression point drops much quicker with current than the gain does [3], so this solution is rarely used in variable envelope protocols as rapid drop in output compression causes the device to move into the non-linear region. However, with constant envelope

modulation this scheme can achieve relatively high efficiencies. The efficiency still suffers at low gains as the impedance of the transistor changes with bias [12].

Combining variable attenuation and variable bias can achieve good results for a variable envelope signal. As bias is lowered, attenuation on the front end is added in order to keep the $P_{1dB,in}$ at a similar or higher level. However, again we see that the variable bias on the final stage causes mismatch for optimum gain and for optimum load-line.

Any of the above systems could be improved either by maintaining the impedance match, or by optimizing the load-line across the various levels of gain. Either of these of will increase the efficiency of the device by increasing power out for a given bias. Whether impedance match or load-line is more important will depend on the modulation scheme of the signal passing through the device, and how the scheme is affected by compression. This thesis however, concentrates on impedance matching more so than load-line optimization.

2.4 Benefits of an Automated Matching Network

Any of the above schemes produce variable input- and output-impedances and variable optimum load-lines as the device is swept through various gain settings. An automated matching network (AMN) can account for the changes in characteristics of the device over its dynamic operating range. Adapting to these impedances as current states are changed will keep the gain high for a given current bias. This will allow devices to operate at a lower bias

for a given gain setting, increasing the efficiency of the PA, and therefore battery-life of the device.

While it is much more difficult to implement, an AMN that adapted to optimum load-line variation would have great benefits. In devices implementing constant-envelope modulation schemes, the devices operate deep in compression. When bias is dropped from the nominal state, the final stage transistor is working far from the optimal load-line for efficiency purposes. In every state other than the maximum output state the device draws much more current than would be required if the load-line could remain matched.

In variable-envelope modulation schemes, dropping bias is much more problematic. These devices normally operate backed off several dB from the 1-dB compression point in order to maintain signal fidelity. When current is dropped from a relatively high density, the output 1-dB compression point drops much faster than the linear gain. Thus the output-signal power will start encroaching into the non-linear region of operation. If automated load-line matching was incorporated, the output P_{1dB} would not drop as fast with respect to current. If gain reduction doesn't compensate for the drop in linearity an AMN on the input can introduce the precise mismatch loss in order to compensate.

If the AMN was continuously adapting, then variations due to environmental variables such as temperature can be compensated for. Many wireless applications give specifications over the $-40^{\circ}C$ to $+85^{\circ}C$. Over such a wide range, transistor characteristics change significantly as carrier-mobilities and carrier concentrations change. Incorporating an AMN into the

device could allow companies to give more stringent specifications to the product. This would result in reducing the necessity for tight controls on other parts of the circuit as they can have more process variation and still maintain overall system specification. This would result in simpler design of other parts of the circuit, and thereby add value to the compensated product.

An additional benefit to wireless applications includes antenna matching in various environments. In mobile applications antenna impedance varies with environment. Setting a laptop down on a surface will change the impedance and result in a change in gain. If the antenna is matched using an AMN, the impedance change would not result in a mismatch loss, although radiation patterns would still be sub-optimal. However, a sub-optimal radiation pattern combined with reduced power transmission will greatly reduce range. By compensating for one of the variables, the deleterious effects will be reduced. Wireless LAN also has similar issues. Placement of metal furniture such as shelves underneath a base-station affects the impedance and radiation pattern of the antenna, and an AMN can account for the change in impedance.

2.5 Project Architecture

In order to match to an unknown impedance, the system must either measure the complex impedance directly, or must use a search algorithm in order to find the load impedance which results in the maximum power output. The first requires an impedance measurement while the second requires only a power measurement. The system then requires a variable matching

network, in this case a voltage-controlled matching network (VCMN) to synthesize the desired match. Figure 2.4 shows these two basic architectures which would be connected to the port to be matched. The tradeoffs are presented in Table 2.1.

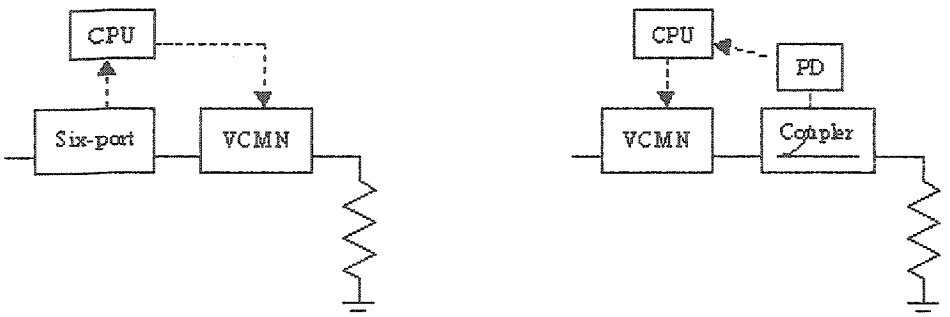

Figure 2.4: Two possible architectures for an AMN (a) six-port (b) single power detector

Table 2.1: Comparison of architectures

Six-port Architecture	**Single Power Detector Architecture**
Complex Architecture	Simple Architecture
Fast (Measure then match)	Slower (Iterative Search)
Large Footprint	Small Footprint
Linear Measurement Only	Linear and Non-linear Measurement
Requires Calibration	Very simple calibration needed

The more complex architecture is a result of the required six-port and four power detectors as opposed to a single power detector. This complexity results primarily in increased size of the circuit, which may result in a prohibitively large chip. Design of the overall topology of the six-port is well documented, however implementing one that is compact is difficult due to the use of couplers and hybrids. Since size scales inversely with frequency for these circuits, the six-port based architecture is more readily adapted to high-frequency systems than low.

The speed at which at a match can be obtained will limit which protocols the AMN can be used for. Some protocols require quick changes in power or frequency at the output, while others have relatively long space between packets. Different protocols require different duty cycles of the output circuit. This will affect the speed requirements of the measurement and matching.

Many of the standards (DOCSIS, WLAN) require that the final stage amplifier work well inside the linear region to maintain signal fidelity. Only those standards that employ constant envelope modulation schemes, such as BlueTooth, allow the PA to be operated in heavily non-linear regions. Thus, the restriction to linear devices in the proposed architecture does not make it impractical for all protocols. However, using this AMN on both ports of a PA is limited to those systems that operate in the linear region, while protocols that are capable of operating in the non-linear region should only use this AMN architecture on the input of the PA if at all.

The calibration algorithm required for a six-port based architecture does not cause any major memory or computational issues, as calibration constants are few and can be stored on the memory available on the vast majority of modules produced. It does however require a repeatable process, or a method of calibrating each AMN chip, whether separate or integrated with other components. Since the passive circuitry of the six-port will vary little over temperature the calibration would only have to be done once per AMN. In fact, as process variation on the passive six-port should be minimal it may be possible to characterize just a

few six-ports and apply it to an entire production lot. With proper use of band-gap circuits the power detectors can also be made very stable over process and temperature.

Looking at the characteristics of the two architectures it appears that each has their advantages. However, as single power detector methods have been experimented with by others [7], this thesis will be of more value if the application of a six-port architecture is explored.

For this project, the six-port architecture was used. Given the tradeoffs it is not initially clear which architecture is better. However, the six-port architecture is chosen for its suitability for applications where the need for speed or reduced processing is paramount.

Chapter 3: The Six-Port Reflectometer

This chapter discusses the metrology involved in the project. It will include general four-port and six-port reflectometer theory, six-port to four-port reduction, and six-port calibration [16-23]. Two-port measurement using dual reflectometers will be discussed, as well as a novel two-port measurement using a reflectometer and a calibrated variable load. A six-port reflectometer will be implemented using off-the-shelf components and tested for repeatability and accuracy. Sources of measurement error are discussed.

Off the shelf components were used to build the six-port. Practical aspects of an integrated six-port implementation will be discussed in detail. However, due to equipment available, no direct testing will be done of the speed of six-port.

3.1 Basic Reflection Measurement Principles

The process of measuring the reflection coefficient, Γ, of a device can be broken down into several basic concepts. Since, the reflection coefficient is the ratio of voltage reflected to voltage incident on a load, we wish to sample both these waves. This can be accomplished using a simple bi-directional coupler as shown in Figure 3.1, with a source port (port 1), test port (port 2) and two measurement ports (ports 3 and 4). Here b_3 and b_4 are the waves at the power measurement ports, b_2 is the wave incident on the measured load and a_2 the wave reflected from the load. The reflection coefficient is then $\Gamma = \frac{a_2}{b_2}$.

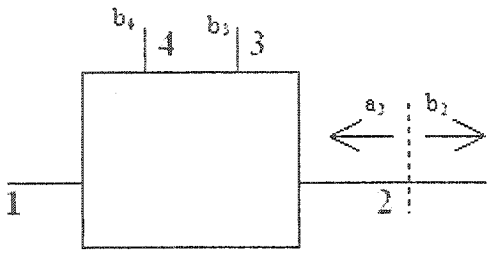

Figure 3.1: Four-port network diagram

If the four-port is an ideal bi-directional coupler (has perfect isolation) then the measurement ports are simply a proportion of each wave, and Γ can be found by simple dividing the two and multiplying by a constant. In practice, the observed powers at each port will be a mix of both incident and reflected waves, and normalized wave amplitudes at the measurement ports become:

$$b_3 = Aa_2 + Bb_2 \tag{3.1}$$

$$b_4 = Ca_2 + Db_2 \tag{3.2}$$

dividing (3.1) by (3.2) to yield a vector indication, w, we get:

$$w = \frac{Aa_2 + Bb_2}{Ca_2 + Db_2} = \frac{A\Gamma + B}{C\Gamma + D} \tag{3.3}$$

then dividing through by D and renaming the constants:

$$w = \frac{d\Gamma + e}{c\Gamma + 1} \tag{3.4}$$

Since the above equation has three complex constants we need three distinct solutions to the above equation in order to solve for said constants. The three constants are found by observing w at three precisely known loads and solving equation (3.4). Once the constants have been found, any unknown load can be measured by finding the value of w and applying the inverse relation.

$$\Gamma = \frac{e - w}{wc - d} \tag{3.5}$$

However, to observe the complex vector w, we need to divide the signals from the two measurement ports using a mixer, usually a super-heterodyne receiver, and any deviation from linearity in the receiver will produce measurement errors. Measurement error due to non-linearity will be greater when loads measured are not near to the standards used for calibration.

The six-port reflectometer is able to duplicate the function of the four-port reflectometer, but uses scalar power measurements instead of vector wave measurements to observe Γ. This avoids the complication of designing a super-heterodyne receiver and the associated linearity issues of the mixers involved, thus simplifying the process greatly. However, reduction of

circuit complexity comes at a cost of greater calibration complexity, though the required number of precisely known standards remains the same.

3.2 Six-port Reflectometer

A six-port reflectometer shown in Figure 3.3 uses four scalar power measurements. Port 1 is the source port, port 2 the test port and the remaining ports are measurement ports. The elimination of the need for phase information simplifies the implementation, and since the junction is passive, the linearity of the system is limited only by the linear range of the power meters employed at the four measurement ports.

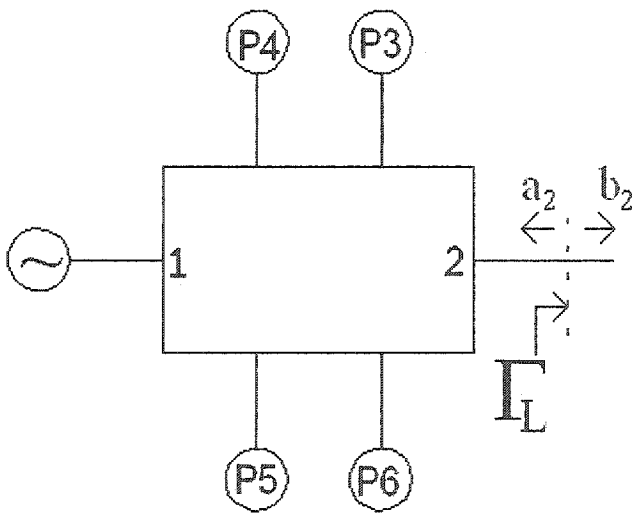

Figure 3.2: Six-port reflectometer diagram

The powered measured at each of the measurement ports is given by:

$$P_i = \left|\alpha_i a_2 + \beta_i b_2\right|^2$$
$$P_i = \left|\alpha_i \Gamma + \beta_i\right|^2 \left|b_2\right|^2 \qquad (3.6)$$

In order to simplify the calculation we redefine our measurements to use port three as a reference. Defining $|w_k|^2$ as the power ratio of P_k/P_3 for $3 < k \leq 6$ yields:

$$|w_k|^2 = \left|\frac{\alpha_k \Gamma + \beta_k}{\alpha_3 \Gamma + \beta_3}\right|^2 \tag{3.7}$$

or

$$|w_k|^2 = \left|\frac{d_k \Gamma + e_k}{c\Gamma + 1}\right|^2 \tag{3.8}$$

The three equations for w_k define three circles in the complex plane, intersecting at Γ. Rewriting (3.8) into the form of a circle gives:

$$\left|\Gamma - \frac{c^*|w_k|^2 - d_k^* e_k}{|d_k|^2 - |c|^2|w_k|^2}\right|^2 = \frac{|w_k|^2 |d_k - ce_k|^2}{\left(|d_k|^2 - |c|^2|w_k|^2\right)^2} \tag{3.9}$$

simplifying:

$$|\Gamma - \Gamma_{0k}|^2 = r_k^2 \tag{3.10}$$

where:

$$\Gamma_{0k} = \frac{c^*|w|^2 - d_k^* e_k}{|d_k|^2 - |c|^2|w|^2}$$

$$r_k = \frac{|w||d_k - ce_k|}{|d_k|^2 - |c|^2|w|^2} \tag{3.11}$$

The equations resulting above have seven complex unknowns, c, d_k, e_k for k = 1,2,3. Calibration then requires seven precisely known loads. This calibration is considerably more complex than the four-port calibration. In order to reduce this complexity, a method referred to as six- to four-port reduction is used.

3.2.1 Q-Points and Measurement

In practice, if our reference port is isolated from the reflected wave (3.6) becomes $P_3 = |\beta_3|^2 |b_2|^2$ and it follows from (3.8) that $c = 0$. In such a case, Γ_0 becomes constant in equation (3.10) for each port and we define the q-points [16] as the center of these circles.

$$q_k = \frac{e_k}{d_k} \tag{3.12}$$

We also note that, to the extent that $c \cong 0$, the radius of the circle is proportional to $|w|$ and the q-point for a given measurement port, can be found by observing Γ when the observed power at that port is zero.

The q-points are of interest in that they relate to the repeatability and accuracy of the measurements. Since the power ratios, w_k, each correspond to a set of solutions described by circles centered on these q-points, the unique solution can be found by finding the intersection of these circles. If the q-points are co-linear, then no unique solution exists. If the q-points are tightly spaced, then small errors in the power measurements can yield large

error on the calculated intersection resulting in low accuracy and repeatability of six-port measurements. It is therefore important that the q-points of the six-port be widely spaced.

3.3 Six- to Four-port Reduction

As mentioned at the end of Section 3.2, the six-port equations developed here require 7 precisely known loads to solve for the characteristics c, d_k and e_k for $k = 1,2,3$. A method refered to as six- to four-port reduction [16] is used to reduce the problem to three unknown complex coefficients, resulting in a final calibration step nearly identical to the four-port reflectometer calibration, and removes the requirement for 7 precisely known loads. The entire calibration then requires 9 loads, but only 3 of which must be precisely known and one approximately known. The unknown loads used in the calibration need only to be distinct.

The four-port reflectometer produces a single vector quantity, w, whereas a six-port generates three scalar quantities $|w_k|$. However we can, using the three scalar quantities, find the vector value of w_1. From the vector form of (3.8), and solving for Γ:

$$\Gamma = \frac{e_1 - w_1}{w_1 c - d_1} = \frac{e_2 - w_2}{w_2 c - d_2} = \frac{e_3 - w_3}{w_3 c - d_3} \qquad (3.13)$$

Solving for w_1 and eliminating Γ we find:

$$|w_1|^2 = |w_1|^2, \quad A^2|w_2|^2 = |w_1 - m|^2, \quad B^2|w_3|^2 = |w_1 - n|^2 \qquad (3.14)$$

We now have three equations in the w_1 plane based on scalar power measurements, $|w_k|^2$. These equations describe circles in the w_1-plane, with centers (0,m,n) which intersect at a single point. The scalar parameters $A^2, B^2, |m|, |n|$ and $|m-n|$ can be found using 9 or more unknown loads. The precise details of this calibration are extensive and thus left in appendix A. This allows w_I to be determined by the 4 power measurements, with a sign ambiguity left in the imaginary part. If we then use the three precision standards for four-port calibration, along with an approximately known standard to resolve a sign ambiguity in w_I, we can fully characterize the six-port reflectometer. The process of find the reflection co-efficient is to measure power at the four ports, calculate w_I and from that find Γ.

Using six- to four-port reduction we can calibrate the reflectometer using 9 or more loads, 3 of which must be precisely known and one approximately known. There is no requirement that the $3\frac{1}{2}$ standards be separate from the 9 loads used in six- to four-port reduction. It is worth noting that the most accurate calibration uses more than 9 loads and uses a least-squared error solution in order to get the calibration constants. [16]

3.4 Two-port Measurements using Dual Six-port Reflectometers

Given that we only require magnitudes for the transmission parameters, we do not need a full calibration. A diagram of a two-port network analyzer incorporating dual six-port reflectometers is shown in Figure 3.4. The phase-shifter in the diagram is required to provide 3 different $\frac{a_1}{a_2}$ values required for the measurement. Readings from the power meter were

retrieved using the GPIB protocol during the thesis, however, an integrating solution would require analog-to-digital converters to communicate the analog power measurement to the controlling unit.

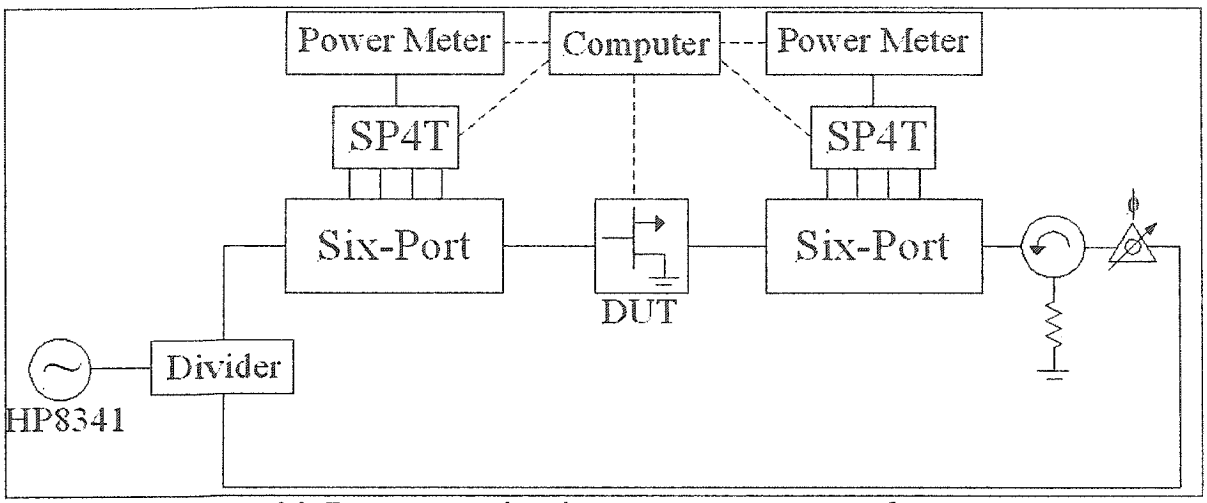

Figure 3.3: Two-port network analyzer incorporating six-port reflectometers

The divider, phase shifter and isolator are required in order to vary the ratio of powers injected into each port of the DUT. The six-ports measure the reflection coefficients under different power ratios and the results can be used to calculate two-port s-parameters.

If we consider the two-port circuit, the observed reflection coefficients, $\frac{b_i}{a_i}$, in terms of s parameters are:

$$b_1 = s_{11}a_1 + s_{12}a_2$$
$$b_2 = s_{21}a_1 + s_{22}a_2 \tag{3.15}$$

$$\rho_1 = s_{11} + s_{12}\frac{a_2}{a_1}$$
$$\rho_2 = s_{22} + s_{21}\frac{a_1}{a_2} \tag{3.16}$$

Solving (3.16) by eliminating $\frac{a_1}{a_2}$, we find:

$$(p_2 - s_{22})(p_1 - s_{11}) = s_{21}s_{12} \tag{3.17}$$

$$p_2 p_1 = p_2 s_{11} + p_1 s_{22} - \Delta \tag{3.18}$$

Using (3.18), we can solve for s_{11}, s_{22}, and Δ by observing p_1 and ρ_2 for three values of $\frac{a_1}{a_2}$.

From (3.16) we can find magnitude of the transmission parameters:

$$|s_{12}| = |p_1 - s_{11}|\left|\frac{a_1}{a_2}\right|$$
$$|s_{21}| = |p_2 - s_{22}|\left|\frac{a_2}{a_1}\right| \tag{3.19}$$

The value of $\left|\frac{a_1}{a_2}\right|$ can be found by adding a power calibration to the six-port calibration.

Returning to the standard reflectometer and using (3.6):

$$P_3 = |\alpha_3\Gamma + \beta_3|^2 |b_2|^2$$
$$P_3 = |\beta_3|^2 |1 + c\Gamma|^2 |b_2|^2 \qquad (3.20)$$

and:

$$P_L = (|b_2|^2 - |a_2|^2)$$
$$P_L = (1 - |\Gamma_L|^2)|b_2|^2 \qquad (3.21)$$

dividing we get:

$$P_L = \frac{1}{|\beta_3|^2} \frac{(1 - |\Gamma_L|^2)}{|1 + c\Gamma_L|^2} P_3 \qquad (3.22)$$

substitute in (3.4)

$$P_L = \frac{1}{|\beta_3|^2} \frac{\left(|d - wc|^2 - |w - e|^2\right)}{|d - ce|^2} P_3 \qquad (3.23)$$

consolidating constants:

$$P_L = K\left(|d - wc|^2 - |w - e|^2\right) P_3 \qquad (3.24)$$

Connecting a power-meter to the test-port the reflection coefficient and power can be measured, resulting in a value for K. This constant can now be used to allow the six-port to measure both reflection coefficient and power out of the circuit port. From the power at the test-port, a value for $|a|$ can be found.

$$P_L = (1 - |\Gamma_L|^2)|b_2|^2 \qquad (3.25)$$

Note, that since b_2 of the single six-port reflectometer represents the outgoing wave, it represents the incident wave $|a|$ on the two-port DUT.

Since each six-port now measures Γ and $|a|$, the values of $s_{11}, s_{22}, s_{21}s_{12}, |s_{21}|$ and $|s_{12}|$ can be found. The phase of the transmission parameters is not important in the determination of gain or loading of the transistor. In Chapter 2 we mentioned that the above parameters were necessary to calculate stability, G_{Tmax}, G_A and G_p values.

3.5 Two-port Measurements using Variable Load

The dual reflectometer method of measuring two-port scattering parameters results in a large circuit. It also requires power to be injected at the output of the DUT, which is not practical in many circuits and would require a complicated switching scheme. If we want to create an automated matching network, AMN, it is desirable to remove this requirement.

A novel method can be used to measure the s-parameters of the DUT. Since the voltage-controlled matching network, VCMN, is a variable load, it can be used to reflect three different power levels back into the device, thus removing the need to inject power at the output through complex circuitry. In addition, by removing one of the six-port reflectometers we can still measure the s-parameters required for stability and normalized gains, g_{Tmax}, g_A and g_P values. This architecture is shown in Figure 3.4, where source, six-

port reflectometer and VCMN layout with respect to the transistor is shown. The VCMN is controlled by the computer through digital-to-analog converters producing the required bias voltage. As noted in Section 2.2, we do not need all the s-parameters of the device to calculate two-port matching parameters for the device. The following system yields measurements for s_{11}, s_{22} and $s_{21}s_{12}$, which are sufficient for calculating stability of the device, and normalized gain under various loads.

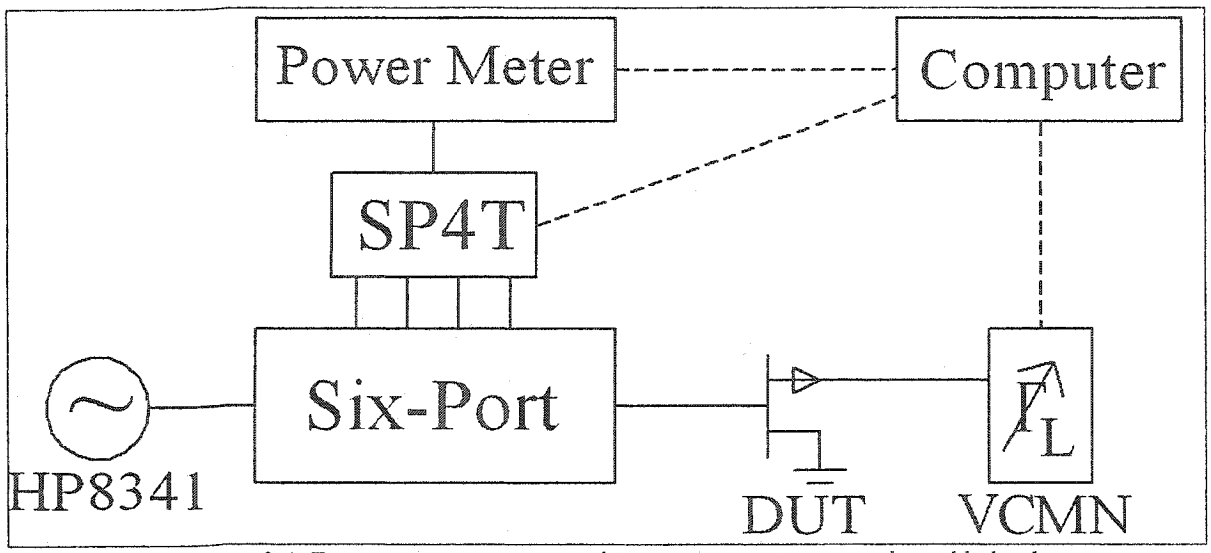

Figure 3.4: Two-port measurement architecture using six-port and tunable load

Measuring two-port loads with a single reflectometer and a calibrated variable load is based on a simple principle. The equation for the input reflection coefficient of a two-port network is:

$$\Gamma_{in} = s_{11} + \frac{s_{12}s_{21}\Gamma_L}{1 - s_{22}\Gamma_L} \tag{3.26}$$

Thus, with three calibrated loads, Γ_L, we can find three unknowns, s_{11}, s_{22} and the product $s_{12}s_{21}$. From this we can calculate Δ, as well as optimum loads for obtaining maximum transducer gain, G_{Tmax}, and loads required to achieve a given gain relative to G_{Tmax}. These same values are also sufficient for determining stability of the device. However, this does not allow us to calculate the actual value of G_{Tmax}. For this we require $|s_{21}|$ and $|s_{12}|$. Note that the three loads produced by the VCMN should be widely separated in order to minimize errors when solving equation (3.26).

While it is obvious from equation (3.26) that scattering parameters can be found using three known loads and performing a one-port measurement, the practical implementation of two-port measurements using a single reflectometer and a variable load does not appear to have been done. This implementation is therefore determined to be novel.

3.6 Implementation of Six-ports

The six-port design was researched, built, optimized for repeatability and speed, measured and then tested for accuracy.

3.6.1 Six-port Design and Assembly

The circuit design was based on the work of Engen [19]. The six-port was implemented using off-the-shelf components. Figure 3.5 shows the layout of the reflectometer, including the six-port broken down into its constituent components. The bi-directional coupler was implemented using two directional couplers. While these off-the-shelf components did not

produce the low loss desired (approximately 2 dB loss at 10 GHz), having bi-directional couplers available would have halved the insertion loss of the six-ports, and the transmission was still sufficient to perform the feasibility tests on the AMN architecture.

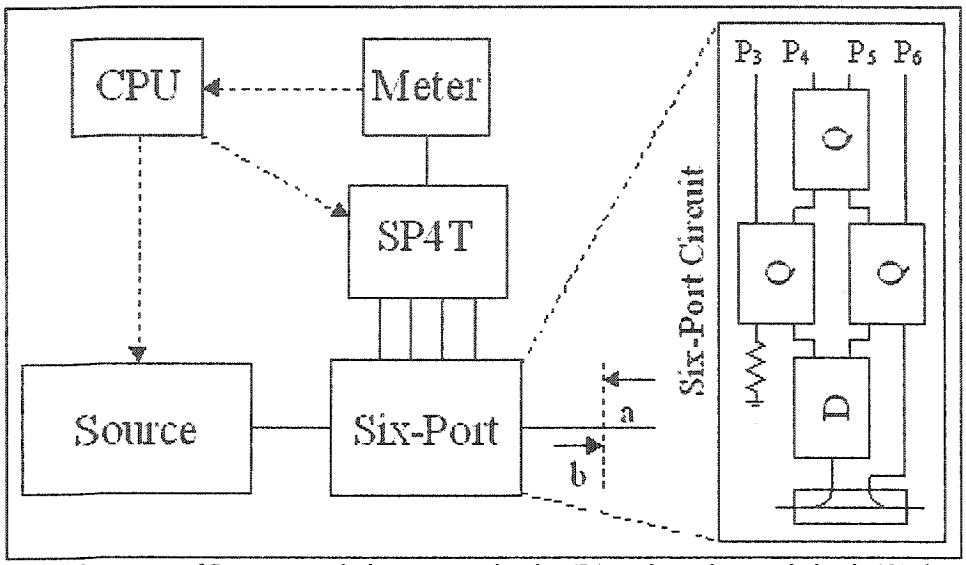

Figure 3.5: Architecture of Six-port, including power-divider (D), and quadrature hybrids (Q) the coupler is implemented using two uni-directional couplers.

Cables in the six-port were semi-rigid SMA. An Anritsu ML2438A Power Meter, and SP4T switch where used to measure power at each of the ports. The system was automated using LabView 5.1 (© 1999 National Instruments.)

3.6.2 Six-port Measurement and Q-point Calculation

The q-points of the circuit in Figure 3.5 can be calculated approximately using ideal components. Assuming all ports except the measurement port are matched, and using

transmission s-parameters for the power divider as $s_{21}=s_{31}=\frac{1}{\sqrt{2}}$ and the hybrid as having $s_{21}=\frac{1}{\sqrt{2}}$ and $s_{31}=\frac{-j}{\sqrt{2}}$ we find the following power at the output ports.

$$
\begin{aligned}
P_3 &= \left|-j\frac{1}{2}k_b b\right|^2 \\
P_4 &= \left|-\frac{1}{2}k_a a+\frac{1-j}{2\sqrt{2}}k_b b\right|^2 \\
P_5 &= \left|-j\frac{1}{2}k_a a+\frac{1-j}{2\sqrt{2}}k_b b\right|^2 \\
P_6 &= \left|\frac{1}{\sqrt{2}}k_a a-j\frac{1}{2}k_b b\right|^2
\end{aligned}
\tag{3.27}
$$

In this case k_a and k_b are the coupling coefficients of the coupler with perfect isolation. Note that P_3 is independent of the reflection co-efficient, making port 3 our reference port. For the remaining ports, finding the reflection coefficient that produces zero power at the port, we find the 3 q-points of the circuit.

$$
\begin{aligned}
q_1 &= \frac{k_b}{k_a}1\angle -45 \\
q_2 &= \frac{k_b}{k_a}1\angle -135 \\
q_3 &= \frac{k_b}{k_a}\frac{1}{\sqrt{2}}\angle 90
\end{aligned}
\tag{3.28}
$$

k_a and k_b will be approximately equal in magnitude, but with different phases. The above architecture has ideal q-points with magnitudes of approximately $(1, 1, \frac{1}{\sqrt{2}})$ with angular separations of (90°, 135°, 135°). However, given phase shifts and non-idealities the absolute angles may be anywhere, but angular separation should be close to the values given. From s-parameter measurements of the six-port, the q-points were calculated and the results can be seen on Figure 3.6. The graph of q-points shows that they maintain wide angular separation, which is important in order to keep error minimized while measuring Γ.

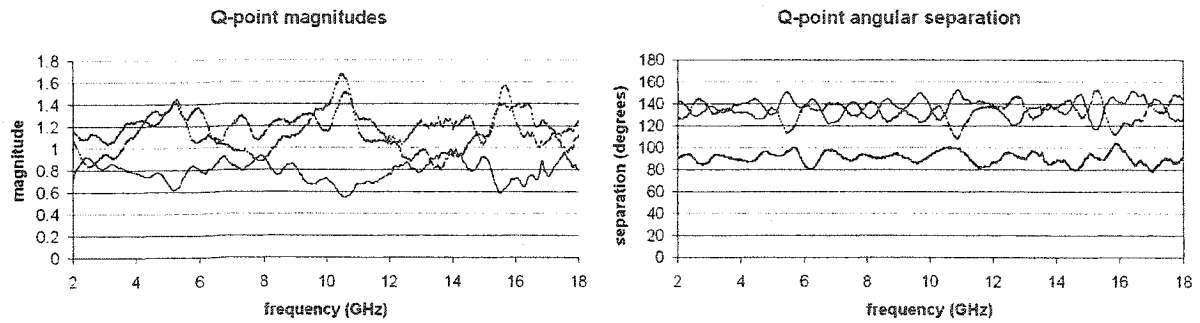

Figure 3.6: q-point magnitudes and angular seperation vs. frequency

The above q-points were calculated by using the assumption that the reference port had nearly perfectly isolation from the reflected wave. Thus the q-point calculation reduced down to equations (3.29).

$$q_1 = \frac{s_{41}}{s_{42}s_{21}}; q_2 = \frac{s_{51}}{s_{52}s_{21}}; q_1 = \frac{s_{61}}{s_{62}s_{21}} \qquad (3.29)$$

3.6.3 Measurement Repeatability and Speed Optimization

In an integrated solution a separate power detector would be hooked up to each measurement port. However, for test purposes one power meter was connected to the six-port via a SP4T switch. Because of the use of a switch, a settle time between switching and power measurement was required in order to assure accurate measurements. In addition the power meter had an averaging function to increase the accuracy.

In order to optimize the performance of the six-port the measurement delay and measurement averaging were varied to increase accuracy with the minimum effect on time. If the delay was too low the circuit didn't settle before the measurement was taken and the number of bad measurements increased. Low averaging of the power measurements caused high variation in low power measurements. Both of these values were increased until no further improvement in measurement was notice from further incrementing of the averaging. This provided high accuracy with out generating intolerably long test times.

3.6.4 System Calibration and Testing

In setting up the circuit, proper procedures were observed for warm-up times of equipment, part cleaning and connection as well as power meter calibration.

The six-port network was calibrated using a total of 12 standards. 8 standards were produced using a phase shifter at 4 different settings, terminated by an open or 3-dB attenuator. The other 4 termination consisted of the approximately known load, a shorted 3-dB attenuator and

the short, open and load standards for standard vector network analyzer, VNA calibration. These 12 standards were used to perform the six- to four-port reduction and then the 3 known and one approximately known used to calibrate the "four-port" constants *c*, *d* and *e*. The reflection coefficient of these twelve loads is shown in Appendix A. After calibrating, the accuracy of six-port was compared to vector network analyzer as shown in Table 3.2. Means and deviations were calculated based on 100 measurements. The definition column in the table was obtained from the documents supplied by HP with the calibration standards. These are the values supplied to the system during calibration.

Table 3.2: Comparison of six-port and HP8510B one-port measurement

Element Measured		Definition	Six-port	HP8510B
Short	Mean	0.9631-j0.2524	0.9642-j0.2492	0.9690-j0.2427
	Standard Dev.		0.0015	0.0003
	Max Deviation		0.0038	0.0006
Open	Mean	-0.9680+j0.2357	-0.9705+j0.2123	-0.9825+j1759
	Standard Dev.		0.0017	0.0005
	Max Deviation		0.0057	0.0010
Load	Mean	0	0.0017-j0.0004	-0.0081-j0.0074
	Standard Dev.		0.0012	< 0.0001
	Max Deviation		0.0034	< 0.0001
3dB Attenuator - unterminated	Mean	NA	-0.2574+j0.0190	-0.2710-j0.0377
	Standard Dev.		0.0018	0.0002
	Max Deviation		0.0040	0.0004

Looking at mean values, it is noted that the six-port is more accurate than the network analyzer, despite the fact that the standard deviation of the measurements was higher. This is best explained as a result of the flexible cable error inherent in the network analyzer measurements. Flexible cable error results from the inability to keep flexible cable fixed

during calibration and measurement. Since the cable characteristics change slightly when moved, the resulting measurements have some error introduced. With the six-port, the only difference between the calibration and measurement phases would have been the uncertainty of connection repeatability between the loads and the six-port network. The network analyzer had two sources of uncertainty, first, the repeatability of connections and, second, the movement of the cables between calibration and measurement. Thus in spite of the fact that more noise existed in the six-port power measurements (resulting in the larger standard deviation) a more accurate measurement was possible.

Error sources for the six-port system consisted of the circuit noise, and repeatability of SMA connections. Drift effects are minimal as the six-port is a passive circuit, which varies little with the room environment. Any drift encountered was most likely due to power meter drift, which was minimized by a long warm-up period. Flex-cable error for the six-port was negligible as cables in the six-port were rigid and the entire setup fixed in position.

The HP8510 had much less noise contributions, however the cables in between the network analyzer and terminations resulted in larger flex-cable error.

3.7 Issues on Integration of a Reflectometer

The large size of the resulting circuit has been mentioned several times. However, the introduction of the multistate reflectometer [23], which uses only a four-port network and two scalar power measurements, provides an alternative to six-port. Its later development in

the literature into a solution that may be automated [24,25] makes it a practical candidate for use as a reflectometer for future automated network matching integrated circuits.

Use of a multistate reflectometer will significantly reduce the size, and half the number of active components required in the power detectors, since fewer detectors are needed. These simplifications come at the cost of additional switching, which must be used to select the various delay lines in the architectures.

As the six-port is primarily passive components, it is easy to integrate it on various technologies. As stable power detectors are required, a band gap circuit may be required. If implemented using a multi-state reflectometer switches are required, however the switches are not along the critical signal path, and the loss introduced by the switches will not effect the circuit adversely.

Chapter 4: Voltage-Controlled Matching Network

This chapter will cover design and implementation of the voltage-controlled matching network, VCMN. The design will be covered from paper calculations, initial simulation methods, design and incorporation of bias-networks and final overall design. Layout and technology issues are also covered.

The fabricated circuit is measured and compared to simulated results. Inconsistencies between actual and simulated performance are discussed and an analysis of design errors is performed.

A brief discussion of the Thru-Reflect-Line (TRL) structures manufactured for measurement of individual components is discussed [24]. Measurement of devices will be shown and a simulation of the matching network with the new models is done in order to check initial simulation errors. The calibration of the VCMN is implemented and briefly discussed.

4.1 Design Goals

The design considerations for a voltage-controlled matching network depend on the application considered. A general purpose circuit, which would be marketed as a chip that could be inserted into any board design to match a wide variety of elements would require the ability to transform a load to a large range of impedances. To increase the number of applications the chip can be used in, a wide range of frequency of use is desirable. This large range of tunable impedances would be offset by the requirement to keep the circuit simple

and minimize the number of elements used. One also requires that the loss of the circuit be minimized. Reducing reflective loss by inserting a voltage controlled matching network has no benefit if the circuit increases resistive losses as a result. Linearity of the circuit over a range of powers is also necessary.

For an application specific design, in which the VCMN will be integrated onto a chip with the elements, most of the requirements are similar. However, because a single application is targeted the impedance-matching range of the circuit can be reduced to only those values that the device in question requires. Also, maximum linear voltage swing on the matching network elements becomes defined. The voltage swing is important if varactor diodes or other active devices are used as the variable impedance as the non-linear nature of the devices will create harmonics if voltage swing is excessive.

It is worth noting that a VCMN could be created which also allows various harmonic frequency matches in addition to matching the fundamental. However, this would greatly increase circuit complexity as well as circuit calibration complexity. It is not the goal of this thesis to implement harmonic matching.

For the purposes of this thesis, the voltage controlled matching network will be a 3rd order circuit designed at 10 GHz in order to maximize Smith chart coverage and minimize loss. Using a 3rd order circuit keeps the circuit simple but still allows a wide range of impedances to be matched. The circuit will be fabricated as an MHMIC on a 10-mil alumina substrate (ε_r

$= 9.2$ and $tan(\delta) = 0.0009$) with gold metalization. The process has air-bridge for spiral inductors, however problems with MIM caps shorting require that the capacitors be implemented with discrete components.

4.2 Circuit Architecture and Ideal Circuit Calculations

Given that we know s_{11}, s_{22} and the product $s_{21}s_{12}$ we can calculate the load required to produce any gain up to g_{Tmax} of the device. To implement a variable gain amplifier, a programmable matching network must be designed to provide a wide range of loads. The two configurations, π- and T-networks, that were examined are shown in Figure 4.1.

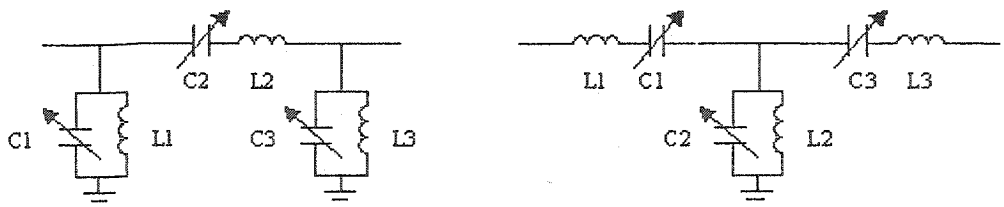

Figure 4.1: π- and T-network schematics

In these circuits, each inductor-variable capacitor pair can be tuned to a range of reactances. A varactor diode acts as the variable impedance and the inductor is used to set the range of tuning for the pair.

The two circuits have similar Smith chart coverage, and similar complexity. However, when considering the implementation of the two, fewer ground vias are required in the T-configuration. Incorporating bias tees for the varactors into the design gives the circuit configuration shown in Figure 4.2. Note that in this circuit L_2 has two functions. First as an

inductor to set the range of admittances which the C_2-L_2 pair may tune to, and as a DC ground for the biasing of all 3 varactor diodes. The series resonant pairs shift the observed load along constant resistance circles on the Smith chart, and the parallel resonant pair shifts the load along constant conductance circles.

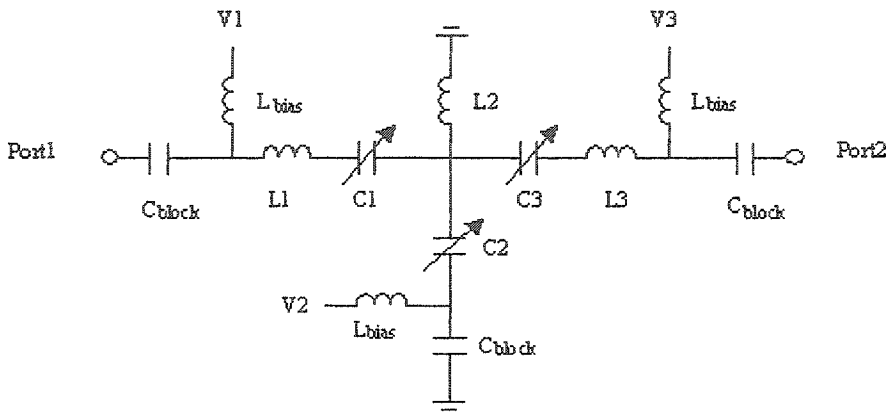

Figure 4.2: T-network schematic including bias networks

4.3 Basic Design

The variable capacitor was implemented using a varactor diode. As a first step each configuration was modeled using ideal elements. The inductors were chosen so each inductor-varactor pair resonated at the mid-point of the range of the varactor's capacitance (C_{min} to C_{max}). By doing this, a large, symmetrical coverage of the Smith chart is obtained. Had the design been for a specific device, the inductor would be chosen to provide optimal coverage for that particular application. As an initial design approximation for inductor

values, ideal components yield the following equations for series (4.1) and parallel (4.2) varactor-inductor pairs:

$$Z_{\min} = j(\omega L - \frac{1}{\omega C_{\min}}) \qquad Z_{\max} = j(\omega L - \frac{1}{\omega C_{\max}}) \qquad (4.1)$$

$$Y_{\min} = j(\omega C_{\min} - \frac{1}{\omega L}) \qquad Y_{\max} = j(\omega C_{\max} - \frac{1}{\omega L}) \qquad (4.2)$$

In order to yield a symmetrical range around open- or short- circuit values, equate $Z_{max} = -Z_{min}$ and $Y_{max} = -Y_{min}$. The resulting inductance values are:

$$L_{parr} = \frac{2}{\omega^2}\frac{1}{C_{\min} + C_{\max}}$$
$$L_{ser} = \frac{1}{2\omega^2}\frac{C_{\min} + C_{\max}}{C_{\min} C_{\max}} \qquad (4.3)$$

Given that we want to maximize the coverage of the Smith chart, we can find optimal values by maximizing Z_{max} or Z_{min}, while maintaining the symmetry imposed by equation (4.3). Substituting (4.3) into (4.1) and (4.2) we find:

$$Y_{\max} = \frac{j\omega}{2} C_{\min} \frac{CR-1}{CR}$$
$$Z_{\max} = \frac{j}{2\omega}\frac{1}{C_{\min}}\frac{CR-1}{CR} \qquad (4.4)$$

where the capacitance ratio, CR is: $CR = \frac{C_{min}}{C_{max}}$

From the above equations, to get the largest range we desire a high capacitance ratio, with C_{min} being high on parallel pairs and minimized on the series pairs. As another criteria, the varactor diode choice must result in realizable inductors.

The diode varactor chosen, Alpha Industries GMV7821, which has a range of 0.19 to 1.93pF, and was chosen for the high CR. The resulting inductor values are realizable in the given technology and are shown below:

$$L_{ser} = 0.73\ nH;\ L_{par} = 0.24\ nH \qquad (4.5)$$

Using the calculated values for inductors and the resulting impedance ranges, coverage for T- and π-circuits was calculated. Assuming zero interconnect length the coverage of the T-network is as shown in Figure 4.3. The Smith chart show possible impedances resulting from sweeping each varactor-inductor pair through 11 evenly spaced impedances or admittances.

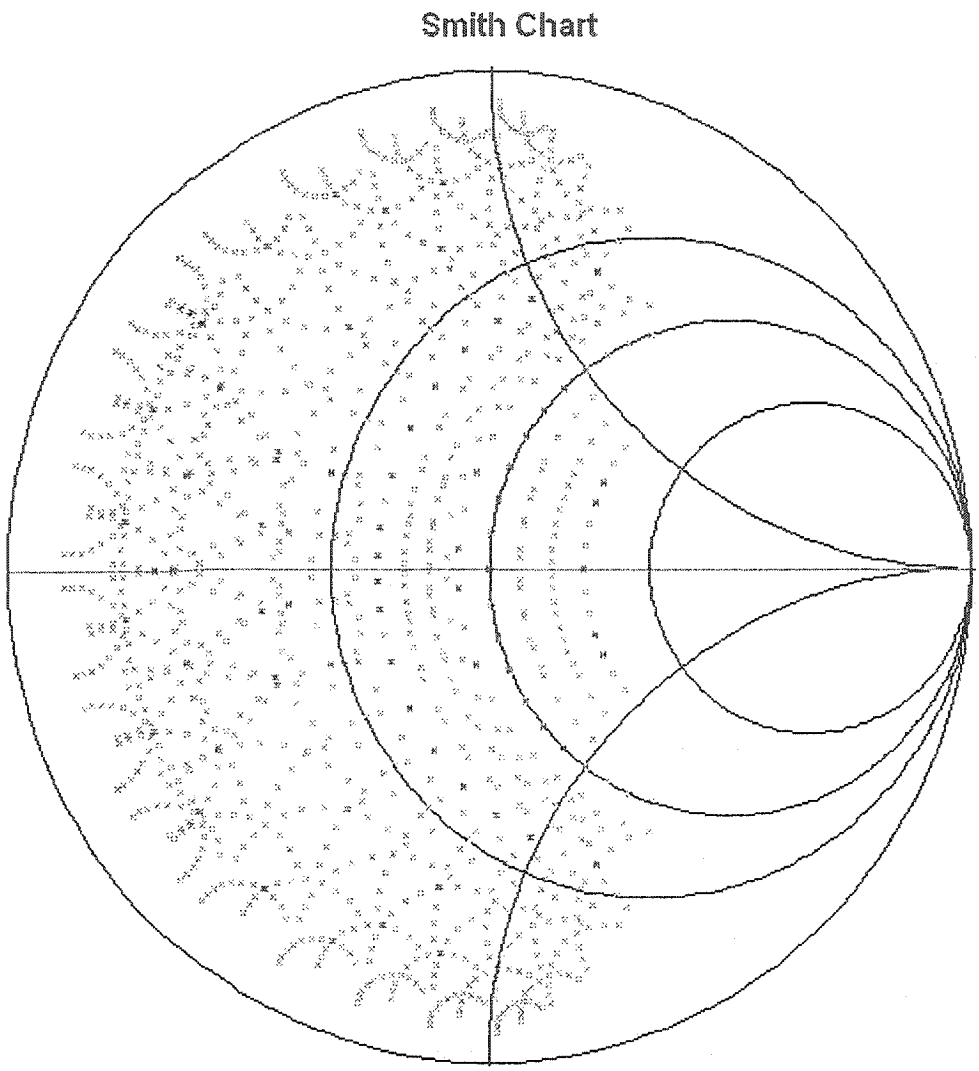

Figure 4.3: Calculated coverage of ideal T-network coverage

The circuit was then refined with models incorporating parasitics and a layout created.

4.4 Circuit Modeling and Layout

To accurately model the circuit, each device had to be simulated in HPADS (© 2001 Agilent) in order to optimize the voltage controlled matching network. The surface mount

components, capacitors and varactors, were modeled from the data sheets supplied by the manufacturer. The integrated components, inductors and interconnects, were modeled based on foundry data. The vias were modeled as a series resistor-inductor pair as described by the foundry data.

The spiral inductors were modeled using field simulation. Initially, spirals identical to those found in the foundry data were modeled using both Momentum (an HPADS software component) and Sonnet (© 1996, Sonnet Software, Inc.). A comparison of the simulated data to the foundry data on spirals showed Momentum to more accurately model the process being used. Based on this the decision was made to use Momentum to design and characterize the spiral inductors for the final AMN circuit. Optimization of the inductors was done by manual iteration, as a suitable optimization process was not available for Momentum. Due to via inductance, only a small trace was required to create the inductor L_2. The spiral inductors used in the final circuit are shown in Figure 4.4.

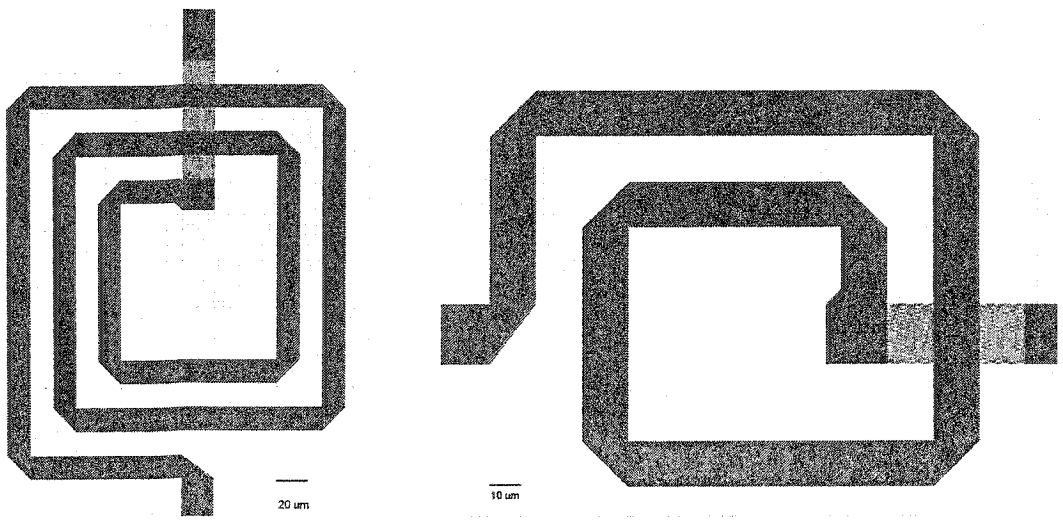

Figure 4.4: Layout of the L_{bias} (left) and L_{series} inductor

While it would have been preferable to measure each component before the design stage, the TRL kit was printed at the same time as VCMN circuit as only one fabrication run was done. In addition, some components were not delivered until after the fabrication of the circuit. The final simulation of the circuit is shown below in Figure 4.5.

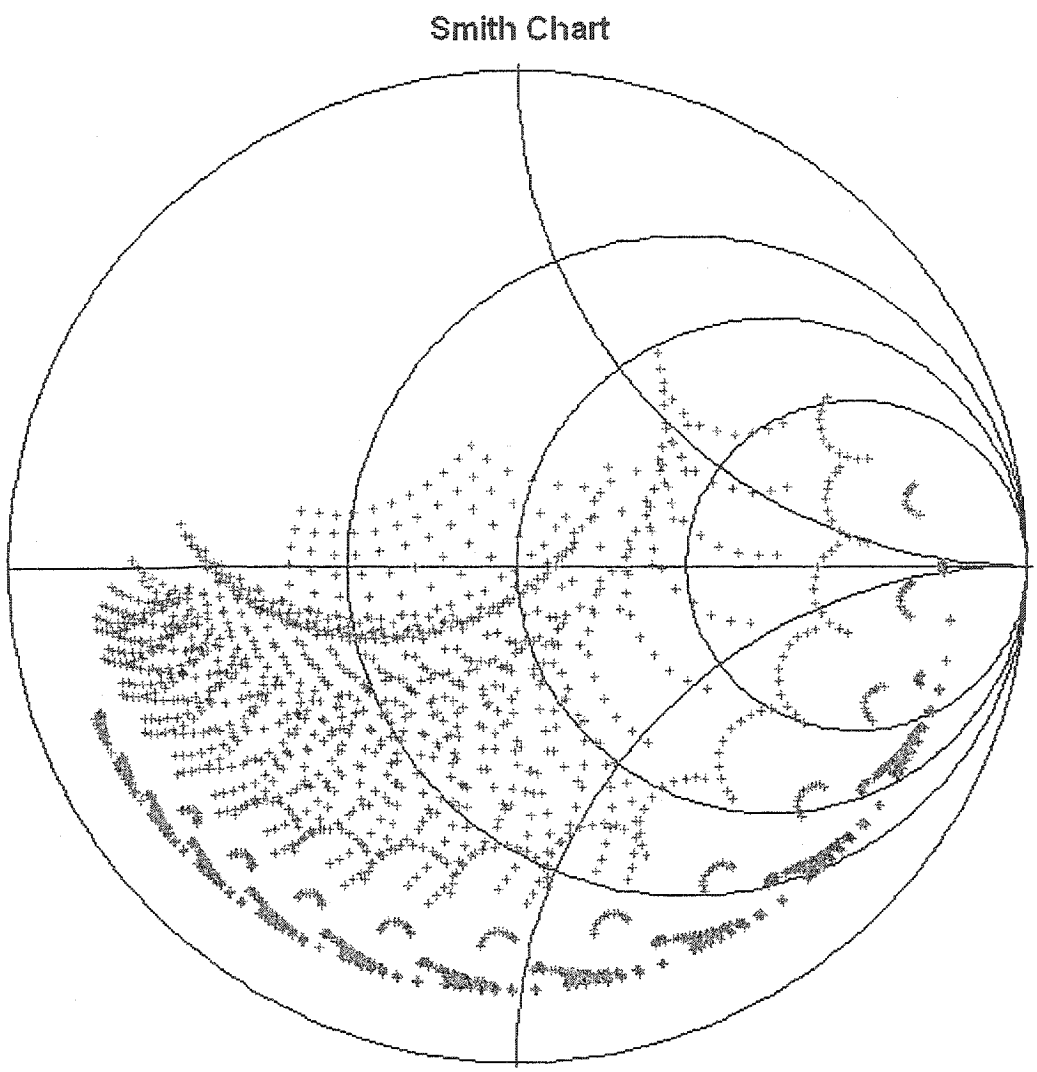

Figure 4.5: Simulated coverage of final layout of AMN with bias networks.

The simulated coverage is close to that of the ideal with the expected phase shift and slight skewing expected from interconnect lengths and various parasitics.

The layout is shown in Figure 4.6, including overall circuit, overall wafer including TRL breakouts, and inductors. The circuit was mounted on a brass test jig with SMA to micro-strip connector for access. When comparing to Figure 4.2, we see that L_1 and L_3 are identical and are referred to below as L_{series}. L_2 has been replaced with via inductance and a short length of line.

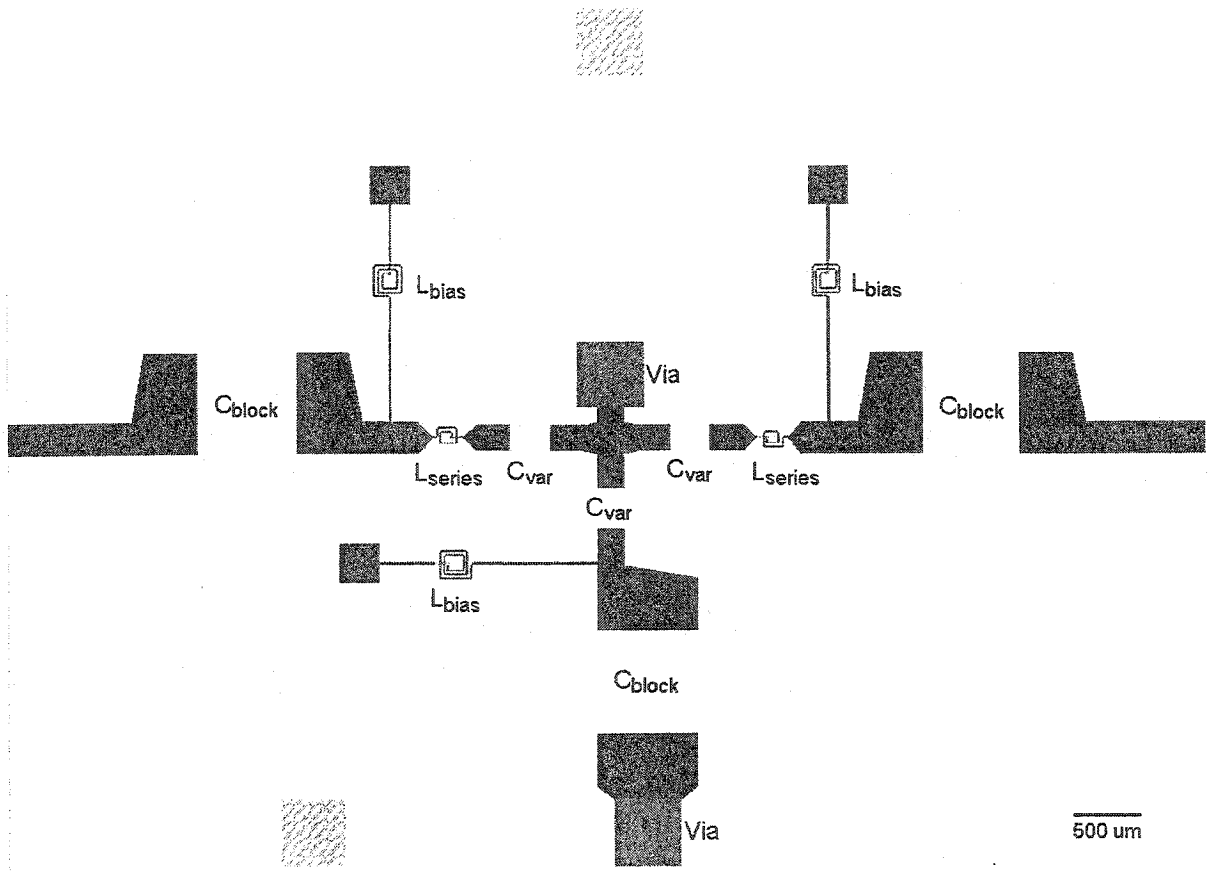

Figure 4.6: Final Layout of VCMN circuit

4.5 Measurement of Voltage Controlled Matching Network

Once the circuit was fabricated and assembled, it was measured. Measurement of the VCMN at several frequencies proved that the largest range of loads could be synthesized at 8.5 GHz. However, at any frequency loss of the circuit could not be brought below 10 dB.

The most likely reason for the difference between simulations with measured component values and reality was most likely due to small errors in the bias circuitry. Further analysis of the bias circuitry showed it was very sensitive to the blocking capacitor and bias inductor values. In addition the DC-bias wires, which were designed to be isolated from the RF signal, were shown to influence the reflection co-efficient when they were disturbed with a metal object. The leakage of RF up the DC bias circuit appears to be the primary cause of loss in the circuit. Measured coverage of the Smith chart is shown in Figure 4.7.

The coverage and loss observed in the actual circuit does not match that found in the simulation. Given the difficulty in modeling the bond wires and DC pins themselves, it may be difficult to simulate this loss in the circuit. In order to account for the discrepancies between the simulation and actual performance, individual components of the circuit were measured and the circuit resimulated.

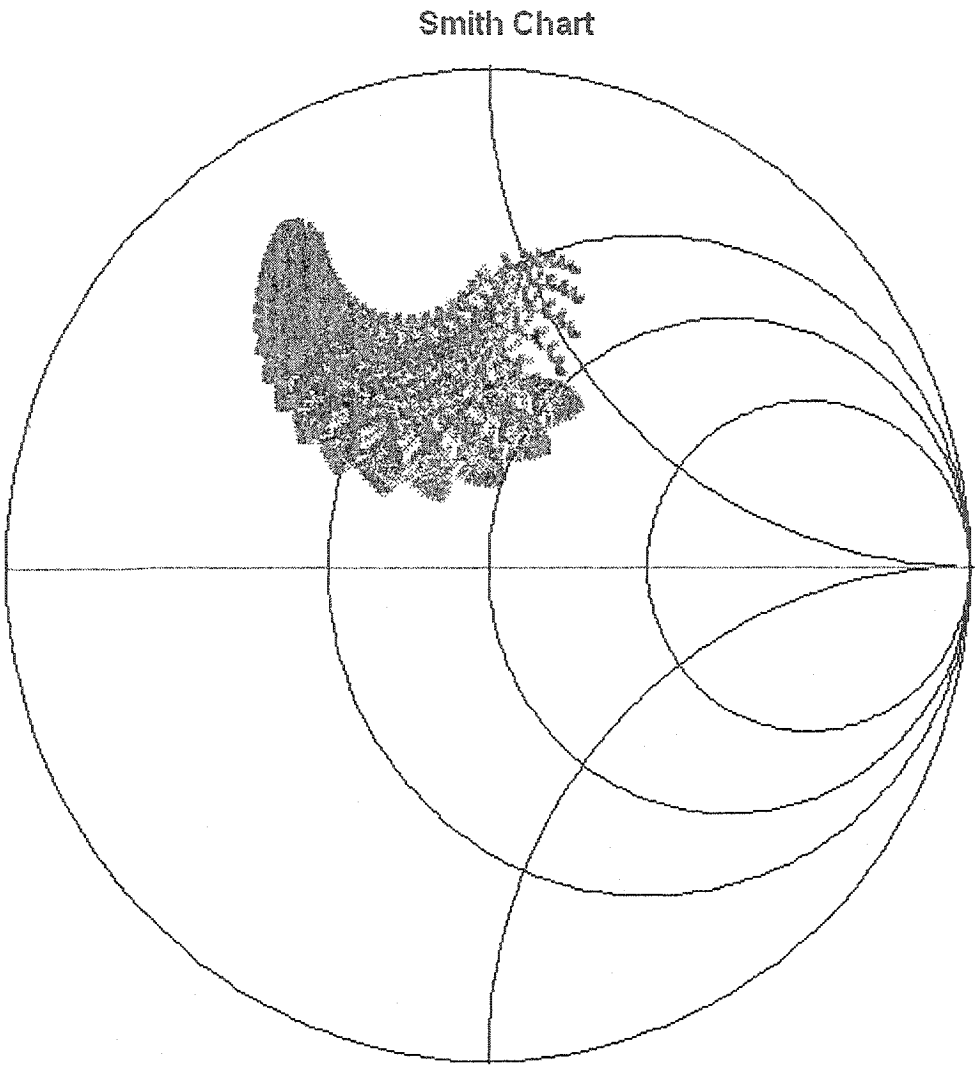

Figure 4.7: Measured coverage of the AMN. The points shown are the calibrated impedances.

4.6 Component Measurement

The capacitors, inductors and via were measured using the TRL standards and the HP8510B. The TRL structures were placed in a WILTRON test jig. The repeatability of the measurements was checked and little variation was encountered provided that the TRL structures were carefully set in the jig.

The blocking capacitor did not meet the specification given and resonated at a much lower frequency than expected. The TRL measurement of the components is summarized in Table 4.1 and Figure 4.8. More detailed results compared to simulation can be seen in Appendix D. As a result the bias tee circuits did not perform as expected, and a fair amount of loss was introduced into the system. The bad isolation of the bias-tee was proven by the alteration of RF performance when metal objects were used to perturb the DC bias port. This suggested that the bias bond-wire also became a part of the RF circuit and probably radiated some power, as it is not a good transmission line.

Table 4.1: ADS Model Information for Various Circuit Components

Element	Simulated (10 GHz)	Measured (10 GHz)
Blocking Capacitor	C = 0.89pF	C = 0.66pF
Varactor Diode	C = 0.2 to 1.9 pF	C = 0.265 to 2.63 pF
Via	L = 150 pH, R = 100 mΩ	L = 124 pH, R = 899 mΩ

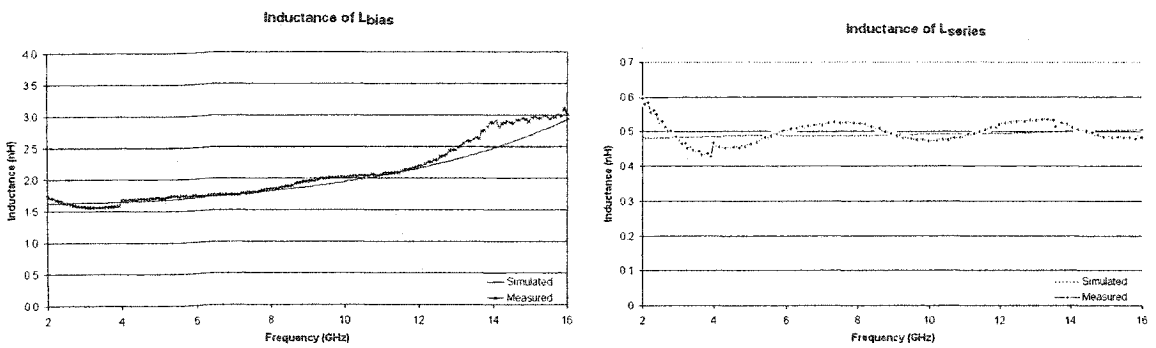

Figure 4.8: Simulated and Measured Inductance for spiral inductors

This severely limited the Smith Chart coverage of the VCMN, and prevented it being used in a gain block. The large losses of the VCMN prevented full realization of the desired amplifier circuit. The VCMN however could still be used to provide a range of loads in order to measure or match to a transistor. Also in Appendix C, it is worth noting that the

capacitance value range of the varactor diodes was shifted, resulting in the coverage of inductor-varactor pairs being moved and shifting the coverage.

Table 4.2 shows loss for the simulated circuit using models versus simulated circuit using measured components. Loss is calculated using $-10\times\log(|s_{21}|^2+|s_{11}|^2)$.

Table 4.2: Simulated loss of circuit with original models and measured models

	Layout Simulation	Simulated with Measured Components
Minimum Loss	1.0 dB	0.77 dB
Maximum Loss	3.3 dB	17.0 dB
Averaged Loss	1.4 dB	2.9 dB

Using the measured s-parameters of the capacitors, inductors, varactor diodes and ground vias, the layout was re-simulated to allow comparison to actual results. The new simulation results are shown in Figure 4.9. Comparing this to the actual performance in Figure 4.7 it is seen that the Smith chart coverage is much more similar, indicating that many of the component parasitics have now been accounted for. The reduced coverage as mentioned is most likely due to capacitor and varactor model inaccuracies. The extremely high maximum loss at a few points (17 dB), is likely due to a resonance within the varactor bias circuit.

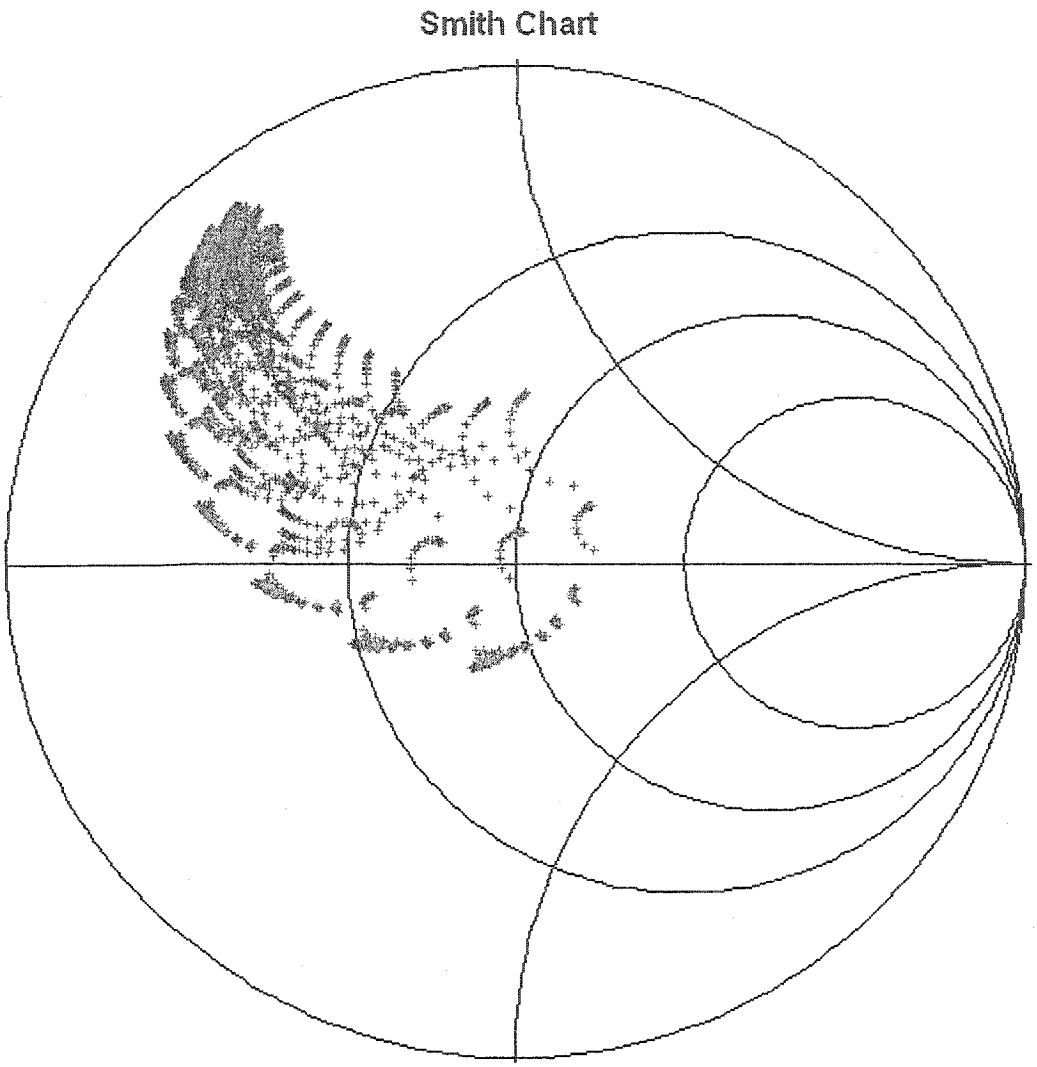

Figure 4.9: Simulated coverage using measured parameters for components

4.7 Calibration of VCMN

Calibration of the VCMN was performed by attaching it to the HP8510B network analyzer, and stepping through bias voltages. A sufficiently dense calibration was achieved by sweeping the voltages from 0 to 10 volts with a 0.5 volt step. The constellation of calibration points is plotted on Figure 4.5 given previously (page 53). Full calibration of the VCMN was

not done with the six-port due to time-constraints. The six-port used a SP4T switch connected to a power meter and thus required significant settle time, leading to extremely long calibrations of the VCMN. Using the HP8510 avoided the excessive setup times.

Calibration of the VCMN at several frequencies proved that the largest range of loads could be synthesized at 8.5 GHz. However, at any frequency, loss of the circuit could not be brought below 10 dB. This made an experiment measuring transducer gain impractical, as a result a test of the ability of the VCMN to match to a g_p value was performed (See Chapter 5).

Chapter 5: System Implementation

This chapter covers the implementation of the overall system containing a transistor amplifier. Two-port measurement of the devices by the system is compared to the measurements from an HP8510 network analyzer. Accuracy of the two-port measurements is investigated.

The system is then used to perform g_p matching. Match achieved versus match desired is compared in order to evaluate precision of the system. Dynamic range achieved is noted, as well as error sources.

5.1 Test Procedure

Due to the losses in the VCMN circuit, the test for the system was not done based on power output. The losses prevented using total gain of the chain including six-port and VCMNs as a method of validation. Instead g_p matching was implemented in order to show feasibility of an automated matching network, AMN. The AMN was implemented using a single six-port and VCMN for measuring the S-parameter of the DUT. As mentioned, this method does not allow for measurement of s_{21} and s_{12} individually; however, this is not required if g_p circles are used. The test does not measure absolute gain but gain relative to maximum gain.

$$g_{P\max} = \frac{1}{|s_{12}s_{21}|}(K - \sqrt{K^2 - 1}) \qquad (5.1)$$

The device was measured at a variety of bias states, and various g_p values were matched for. The match required was found by calculating the g_p circles described by $|\Gamma_L - C_P| = R_P$. Where C_p and R_p are given by:

$$C_P = \frac{g_P C_2^*}{1 + g_P\left(|s_{22}|^2 - |\Delta|^2\right)}$$
$$R_P = \frac{\sqrt{1 - 2K|s_{12}s_{21}|g_P + |s_{12}s_{21}|^2 g_P^2}}{1 + g_P\left(|s_{22}|^2 - |\Delta|^2\right)} \qquad (5.2)$$

For each value of g_p the Γ_L selected was at the point of the g_p-circle nearest 50 Ω. The resulting reflection coefficient is shown in equation (5.3).

$$|\Gamma_L| = |C_P| - R_P$$
$$\angle\Gamma_L = \angle C_P \qquad (5.3)$$

The value calculated above was then used to set the impedance of the VCMN. The input impedance to the DUT was then measured to test whether the correct g_p value had been obtained.

5.2 System calibration and set-up

The calibration of the system for the g_p measurements was always performed right before the measurements in order to provide maximum accuracy. The calibration procedure is listed step-by-step here.

As in the case of the six-port measurement setup, the entire system was allowed to warm-up for at-least an hour. The six-port was then calibrated as described in Section 3.6, including power meter calibration and 12 loads. The VCMN calibration was done as described in Section 4.7.

Three reflection coefficients were chosen to be the calibrated loads for two-port measurement as described in Section 3.5. The three loads were chosen to be as widely spaced as possible in order to minimize the error in solving equation (3.26). If the three data-points used in calibration are similar, an ill-conditioned matrix results, producing large errors when the solution is found. The loads chosen are shown in Figure 5.1 below.

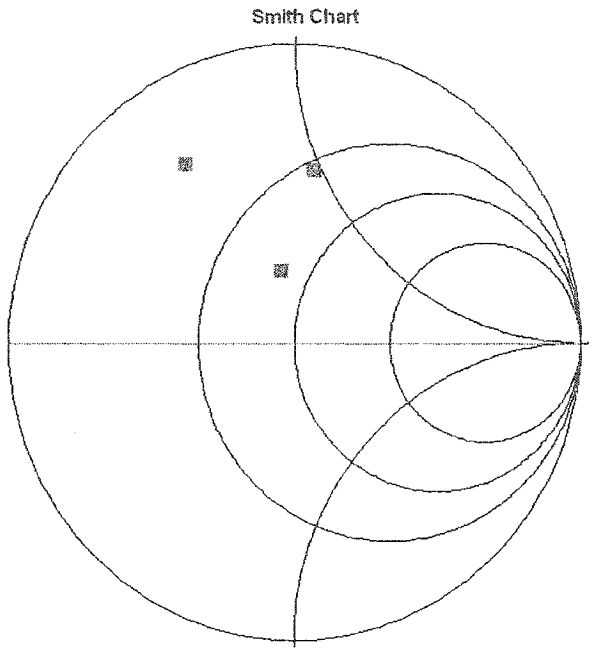

Figure 5.1: Impedance of 3 calibrated VCMN loads for two-port parameter measurement

The system was set up as for two-port measurement as in Figure 3.4 (page 34). The DUT, a NE761, was placed in a Wiltron Universal Test Fixture, and biased. The system did a two-port measurement on the device, determined the match to produce g_{pmax}, the VCMN was programmed to the Γ_L value closest to the required match. The six-port then measured the resulting input impedance of the FET to determine if it was consistent with the desired Γ_L and g_p. The desired g_p was then dropped by 1 dB and the process repeated. The process of matching to different g_p circles was continued until the AMN was unable to produce the load desired.

This was done for several bias points. V_{DS} was set to 6 V and 8 V and ID stepped from 60 to 120 mA in 10 mA steps. The entire process was repeated five times in order to determine repeatability.

5.3 Measurements

The s-parameters gathered from the procedure were compared to s-parameters gathered from the HP8510B network analyzer. See Figure 5.2 for the comparison. The parameter that is measured with the greatest error is s_{22}. Other than that the s-parameters measured by the six-port and the vector network analyzer appear to be in close agreement. In terms of the S_{11} measurement, it is difficult to determine whether the six-port or VNA is more accurate, as flexible cable error is introduced with the VNA, while the six-port calculates the s-parameters as a solution to three measurements which have larger variance between individual measurements than the VNA measurements.

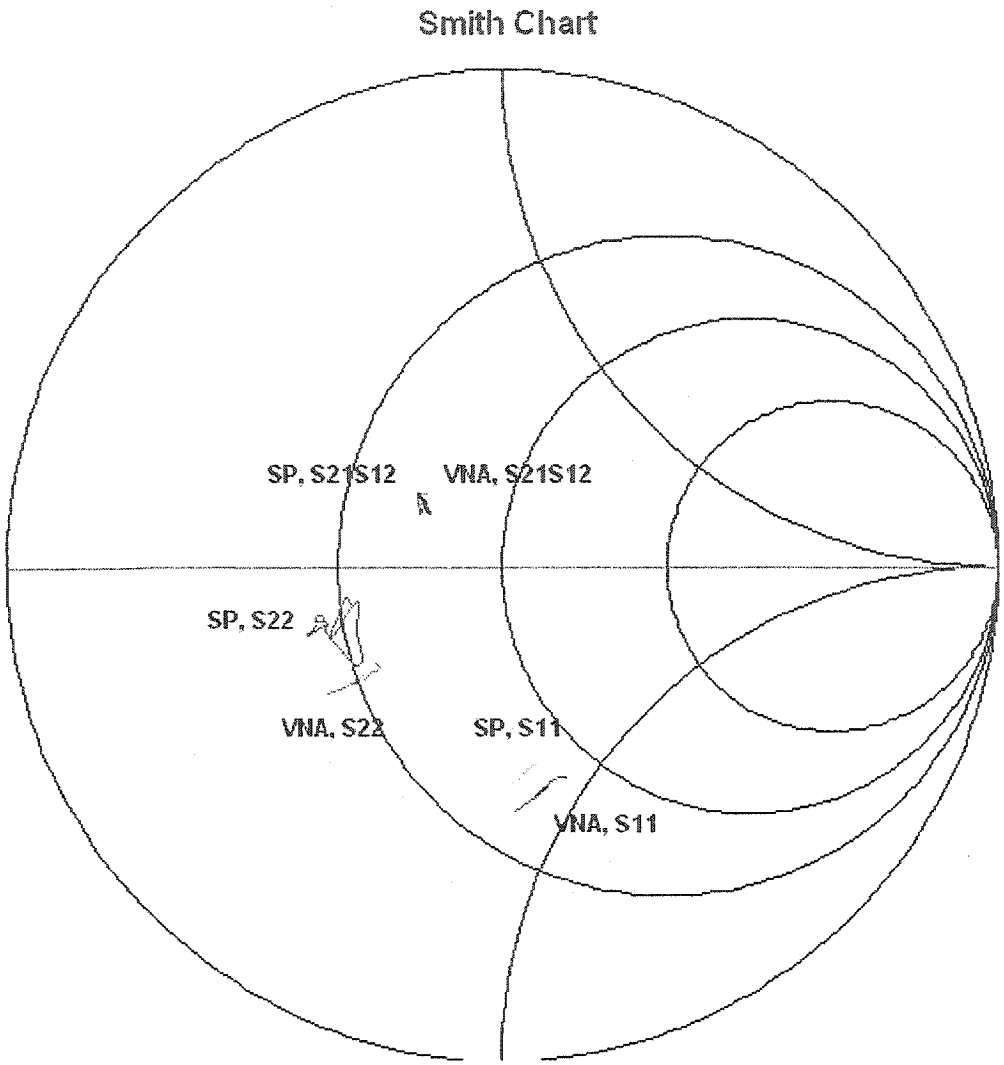

Figure 5.2: S-parameter measurements using the six-port (SP), and HP8510B (VNA)

The g_p matching results are shown in the tables in Figure 5.3. The figure includes a dotted line representing g_p Attained identical to g_p Desired. Deviations of the measurement from the line represent the error in the AMN system. The system was able to provide 5 dB dynamic range for two bias conditions. All data gathered from the test can be seen in Appendix D. Had the VCMN had coverage as designed, the dynamic range for each bias

state would have been improved greatly. Also the system would have been able to match down to much lower bias states, also increasing the dynamic range of the overall system.

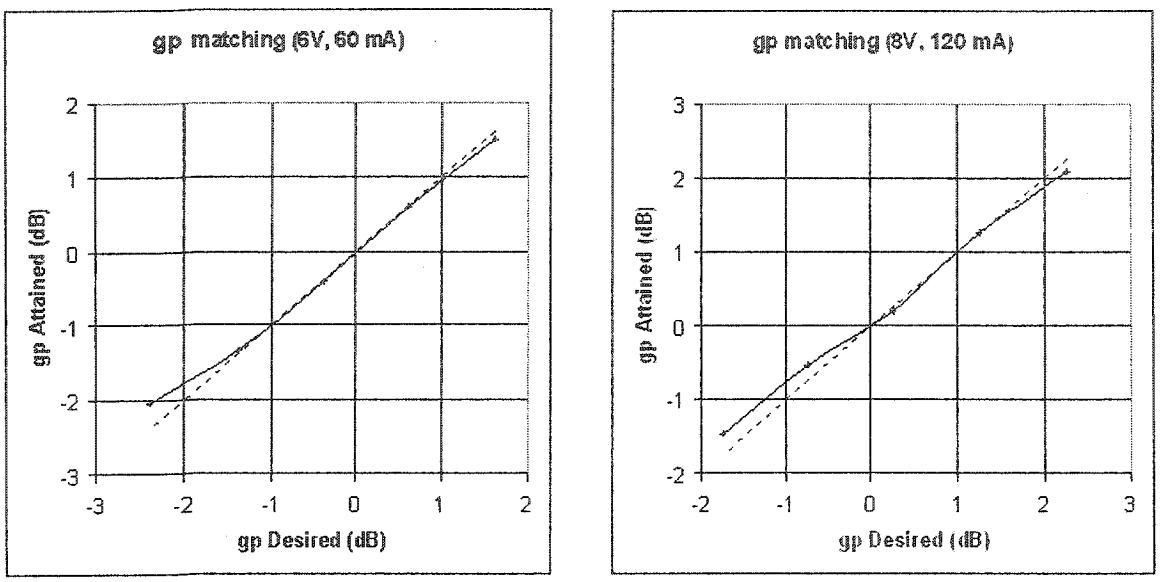

Figure 5.3: g_p measurements averaged over 5 measurements for2 biases

From Figure 5.3, we can see that a 4 dB range was achieved, even with the reduced coverage of the VCMN circuit. If the design had the Smith chart coverage as simulated then the dynamic range would have been much greater.

Chapter 6: Conclusion and Proposals for Future Work

Overall the project was successful. A circuit capable of measuring impedances was built, and a tunable matching network was designed and fabricated capable of synthesizing various loads. The two circuits were combined to produce a novel automated matching method for a device. This thesis proved the feasibility of an automated matching network.

The issues remaining to be solved before a commercial application can be considered are size and loss of the six-port and excessive loss in the voltage controlled matching network. Loss in the six-port could be reduced by using a bi-directional coupler, as opposed to two uni-directional couplers. The size of the six-port was due to the use of broadband off the shelf components. An integrated circuit implementation of the six-port would greatly reduce size, especially if a narrow-band system was desired. In the case of very narrow-band applications the six-port could be composed of lumped elements, as opposed to a transmission line implementation, greatly reducing circuit size again.

The voltage controlled matching network can be improved through a more rigorous simulation phase with device models based on real world measurement. With improved device models the circuit will easily achieve lower loss, and improved Smith chart coverage. The removal of the losses and decreased six-port footprint will allow the manufacture of a practical automated matching network.

In the end, six-port metrology was reviewed and implemented, a voltage controlled matching network was designed and implemented, and the two circuits were combined to produce a circuit that automatically matched to various gain levels. Information on metrology is discussed that allows for a circuit that also allows the measurement of absolute gain of the matched circuit.

Six-port metrology was reviewed in order to give a grasp of the issues involved in implementing the AMN. The mathematics behind six-port reflectometry were discussed in order to provide an understanding of the assumptions and principles behind it. The six-port was implemented and measured. It was found that the six-ports built met specifications and q-points were distributed as expected.

Next the theory, design and implementation of a voltage controlled matching network was investigated. The VCMN provided a continuously variable impedance over a fair range. The simulation results predicted a circuit with good potential for the automated matching network. The simulation used models based on the little data available. While the resulting circuit had excessive losses, it still produced a circuit with sufficient Smith chart coverage in order to implement a prototype automated matching network. This circuit goes to prove the feasibility of creating a variable matching network based around continuously variable impedances.

The implementation of the AMN successfully matched a device for various normalized gain values. While losses prevent total through gain from being measured, the improvements

discussed for the circuit design will allow a true variable gain amplifier to be implemented. This thesis proves the feasibility of the AMN in principle, and a firm base for further work is established for future AMN designs.

AMNs show the possibility of being practical circuits in future products. They have the potential to add value to many chip designs for wireless applications. The realization of practical variable capacitors in MEMS technology will greatly increase the value of these circuits in higher power applications. Improved matching of circuits and the resulting gain in efficiency would benefit the communication links currently in use.

6.1 Designing an Integrated Narrowband AMN

It is desirable that the next step, integrating the entire circuit be completed as a proof of concept. For designing an integrated circuit, a narrow-band solution should be implemented. Broadband circuits will be prohibitively large as the increased bandwidth is achieved by using distributed elements and high-order circuits. Designing for narrow-band will reduce the size of the six-port couplers and dividers and quadrature-hybrids. A narrow-band design can also use several size reduction techniques by using lumped element equivalents to produce the distributed elements in the six-port.

The VCMN does not require components that are uncommon to most processes. A thick top level metal is required for low-loss integrated inductors. Capacitors are required but are common in fabrication processes. The largest obstacle to full integration is the requirement

of a tunable capacitor with a large capacitance ratio. This requires advancement in current varactor diode manufacturing or MEMS tunable capacitors that can be integrated with the other components. Given that harmonic generation would be undesirable in the applications for which this VCMN have been considered, tunable capacitors from MEMS technology is preferred over varactor diodes, as the latter would restrict use to small signal applications.

The primary problem of integrating the solution however will be to come up with a valid calibration technique. The process variation of the varactors may rule out the use of standard calibration table for all chips, as chip-to-chip or wafer-to-wafer variation would make it too inaccurate, so an in-situ method may have to be devised.

A successful design will allow full path gain of an amplifier and AMNs to be tested under various device bias conditions. A successful design will also have increased dynamic range and allow for testing total cascaded gain of an input VCMN, six-port, transistor and output VCMN. Such a test will further validate the practicality of viable commercial uses for an AMN.

6.2 Using VCMN with Power Detector

Use of the six-port, while novel, is a major weak point in the design if it is ever to become commercially viable. The six-port footprint area is prohibitive, and any losses in the bi-direction coupler add noise, reduce efficiency and also reduce the adaptability of the AMN. An AMN that covers a large area of the Smith chart has the advantage that it is applicable to

many more circuits, and a common design could be used across a variety of chips, or a AMN on a chip could be sold for use as an add-on to many circuits.

To reduce the area consumed by the six-port and the losses it incurs, a power detector could be incorporated at the output-port of the AMN and power out would become the control signal for the automation of the matching network. This would lead to a similar topology as in the paper by Vai and Prassad [7], but with the advantage of more adaptability provided by continuously tunable impedance over switch impedances.

For this control structure to work, a search algorithm would have to be developed to quickly adapt to changing loads, and find maxima reliably. Because this topology returns less information to the control unit it is less flexible and care must be taken when used with potentially unstable devices.

However this topology also overcomes many of the problems of calibrating an integrated solution. Firstly because with the use of band-gap circuits a power detector can be made reasonably consistent over temperature and process. Secondly, for a search algorithm to find power maxima, the only requirement for the power detector output is that it be monotonically increasing over the range of power outputs to be measured.

The small size and the removal of the need for complex calibration would allow such a circuit to be used in high volume production of commercial products. Of any of the

topologies discussed in this paper, it is the opinion of the author that this one holds the most promise for future use.

6.3 Load-Line Matching

This thesis looked at linear gain matching of a device. However, the output matching of a PA is often chosen for optimum power and not optimum gain. The VCMN could be used for load-line matching in future experiments.

Many amplifiers for wireless applications are built to work on a given supply voltage, depending on typical batteries used for the application. Many of these amplifiers also incorporate current bias circuits that are very consistent with process. In such a case, a calibrated AMN could be integrated on to the back-end of the PA that would maintain a near optimum load-line across all the bias settings. This would have the benefit that an A-class power amplifier could achieve maximum linearity for a given bias regardless of gain-state.

If the circuit actually monitored the bias voltage and current, the AMN could be made to more accurately maintain an optimum load-line. Experiments could be performed with a device bias being measured by an Ammeter and a Voltmeter. The bias state could be used by a control unit to set the impedance of the load. Gain and linearity could be simultaneously determined for different biases as both input match and load-line can be set. Use of AMN on the input could be used to set gain, with bias and the AMN on the output used to set output

power. After this concept is tested, the voltmeter and ammeter could be removed and an attempt made at an integrated solution.

The final circuit could be implemented with an output AMN which ensures maximum linearity for a given bias, and an input AMN which sets the overall gain, thus allowing the amplifier to set gain and linearity independently.

Appendix A. Six-port to Four-port Reduction

In order to simplify calibration, a six-port can be reduced to a four-port network. The four-port network yields a vector, which is related to the reflection co-efficient by:

$$\Gamma = \frac{e - w}{cw - d} \tag{A1}$$

The six-port network yields 3 such vectors; however the use of scalar power measurements means that only the magnitude of the w vector is known. To simplify the six-port measurement we wish to reduce the four power measurements to an equation in a similar form to (1). The equation describing the six-port measurement is taken from equation (3.13):

$$\Gamma = \frac{e_1 - w_1}{cw_1 - d_1} = \frac{e_2 - w_2}{cw_2 - d_2} = \frac{e_3 - w_3}{cw_3 - d_3} \tag{A2}$$

Using $Q_k = |w_k|^2$ and solving each Q_k in term of w_1 we get three equations describing circles in the w_1 plane.

$$Q_1 = |w_1|^2 ; A^2 Q_2 = |w_1 - m|^2 ; B^2 Q_3 = |w_1 - n|^2 \tag{A3}$$

with:

$$A = \left| \frac{ce_1 - d_1}{ce_2 - d_2} \right| \qquad m = \frac{d_1 e_2 - d_2 e_1}{ce_2 - d_2}$$
$$B = \left| \frac{ce_1 - d_1}{ce_3 - d_3} \right| \qquad n = \frac{d_1 e_3 - d_3 e_1}{ce_3 - d_3} \tag{A4}$$

The three circles described in (A3) intersect at a single point in the w_1 plane. The only condition under which the intersection is not unique occurs when the centers of the circles (0,*m*,*n*) lie on a single line. In practice this is not likely to happen, but should be checked against to ensure errors do not arise during six-port measurements.

Replacing the vector w_1 with rectangular co-ordinates and defining the centers m and n in polar co-ordinates yields:

$$w_1 = u_1 + jv_1; m = M\cos\mu + jM\sin\mu; n = N\cos\nu + jN\sin\nu \tag{A5}$$

$$Q_1 = u_1^2 + v_1^2$$
substitute into (A3): $A^2 Q_2 = (u_1 - M\cos\mu)^2 + (v_1 - M\sin\mu)^2$ (A6)
$$B^2 Q_3 = (u_1 - N\cos\nu)^2 + (v_1 - N\sin\nu)^2$$

Calculating the distance between the centers of the three circles and defining them as p, q and r:

$$
\begin{aligned}
p &= |m-n|^2 = M^2 + N^2 - 2MN\cos(\nu-\mu) \\
q &= |n|^2 = N^2 \\
r &= |m|^2 = M^2
\end{aligned}
\tag{A7}
$$

Now the distances p, q and r are functions of the centers positions which are independent of Γ. In addition, the constants A^2 and B^2 in equations A3 and A6 are also independent of Γ, and are thus characteristic of the six-port network. Rewriting A6:

$$
\begin{aligned}
A^2Q_2 - Q_1 &= (u_1 - M\cos\mu)^2 + (v_1 - M\sin\mu)^2 - (u_1^2 + v_1^2) \\
&= -2Mu_1\cos\mu - 2Mv_1\sin\mu + M^2
\end{aligned}
\tag{A8}
$$

similarly: $$B^2Q_3 - Q_1 = -2Nu_1\cos\nu - 2Nv_1\sin\nu + N^2$$

or:
$$
\begin{bmatrix} \cos\mu & \sin\mu \\ \cos\nu & \sin\nu \end{bmatrix}\begin{bmatrix} u_1 \\ v_1 \end{bmatrix} = \begin{bmatrix} (M^2 - Q_1 - A^2Q_2)/2M \\ (N^2 - Q_1 - B^2Q_3)/2N \end{bmatrix}
\tag{A9}
$$

invert:
$$
\begin{bmatrix} \cos\mu & \sin\mu \\ \cos\nu & \sin\nu \end{bmatrix}^{-1} = \frac{1}{\cos\mu\sin\nu - \cos\nu\sin\mu}\begin{bmatrix} \sin\nu & -\sin\mu \\ -\cos\nu & \cos\mu \end{bmatrix}
$$

$$
\begin{bmatrix} \cos\mu & \sin\mu \\ \cos\nu & \sin\nu \end{bmatrix}^{-1} = \frac{1}{\sin(\nu-\mu)}\begin{bmatrix} \sin\nu & -\sin\mu \\ -\cos\nu & \cos\mu \end{bmatrix}
$$

$$
\begin{bmatrix} u_1 \\ v_1 \end{bmatrix} = \frac{1}{\sin(\nu-\mu)}\begin{bmatrix} \sin\nu & -\sin\mu \\ -\cos\nu & \cos\mu \end{bmatrix}\begin{bmatrix} (M^2 - Q_1 - A^2Q_2)/2M \\ (N^2 - Q_1 - B^2Q_3)/2N \end{bmatrix}
\tag{A10}
$$

In order to simplify equation A10, three new constants are defined.

$$\alpha = \frac{p-q-r}{2\sqrt{qr}}$$
$$\beta = \frac{r+Q_1-A^2Q_2}{2\sqrt{r}} \qquad \text{(A11)}$$
$$\gamma = \frac{q+Q_1-B^2Q_3}{2\sqrt{q}}$$

thus:

$$\alpha = -\cos(\nu-\mu)$$
$$\beta = \frac{M^2+Q_1-A^2Q_2}{2M} \qquad \text{(A12)}$$
$$\gamma = \frac{N^2+Q_1-B^2Q_3}{2N}$$

and A10 becomes:

$$\begin{bmatrix} u_1 \\ v_1 \end{bmatrix} = \frac{1}{\sin(\nu-\mu)} \begin{bmatrix} \sin\nu & -\sin\mu \\ -\cos\nu & \cos\mu \end{bmatrix} \begin{bmatrix} \beta \\ \gamma \end{bmatrix} \qquad \text{(A13)}$$

using: $Q_1 = u_1^2 + v_1^2 = \begin{bmatrix} u_1 & v_1 \end{bmatrix} \begin{bmatrix} u_1 \\ v_1 \end{bmatrix}$

$$Q_1 = \begin{bmatrix} \beta & \gamma \end{bmatrix} \begin{bmatrix} \sin\nu & -\cos\nu \\ -\sin\mu & \cos\mu \end{bmatrix} (\sin(\nu-\mu))^{-2} \begin{bmatrix} \sin\nu & -\sin\mu \\ -\cos\nu & \cos\mu \end{bmatrix} \begin{bmatrix} \beta \\ \gamma \end{bmatrix} \qquad \text{(A14)}$$

using A12:

$$Q_1 = \begin{bmatrix} \beta & \gamma \end{bmatrix} (\sin(\nu-\mu))^{-2} \begin{bmatrix} 1 & \alpha \\ \alpha & 1 \end{bmatrix} \begin{bmatrix} \beta \\ \gamma \end{bmatrix}$$

$$Q_1 = (\sin(\nu-\mu))^{-2}\left(\beta^2+\gamma^2+2\alpha\beta\gamma\right)$$

$$Q_1 = \frac{\left(\beta^2+\gamma^2+2\alpha\beta\gamma\right)}{1-\alpha^2} \qquad \text{(A15)}$$

substituting equation A12 into A15 gives:

$$Q_1 = \frac{\left(r+Q_1+A^2Q_2\right)^2/(4r)+\left(q+Q_1+B^2Q_3\right)^2/(4q)+(p-q-r)\left(r+Q_1+A^2Q_2\right)\left(q+Q_1+B^2Q_3\right)/(8qr)}{1-(p-q-r)^2/(4qr)}$$

$$Q_1 = \frac{2q\left(r+Q_1+A^2Q_2\right)^2+2r\left(q+Q_1+B^2Q_3\right)^2+(p-q-r)\left(r+Q_1+A^2Q_2\right)\left(q+Q_1+B^2Q_3\right)}{8qr-2(p-q-r)^2}$$

$$pQ_1+qA^4Q_2^2+rB^4Q_3^2+(r-p-q)A^2Q_1Q_2+(q-p-r)B^2Q_1Q_3+(p-q-r)A^2B^2Q_2Q_3+\ldots$$

$$p(p-q-r)Q_1+q(q-p-r)A^2Q_2+r(r-p-q)B^2Q_3+pqr=0$$

By defining a new set of parameters it becomes obvious that the above equation can be solved based on nine unknowns.

$$X_1Q_1^2+X_2Q_2^2+X_3Q_3^2+X_4Q_1Q_2+X_5Q_1Q_3+X_6Q_2Q_3+X_7Q_1+X_8Q_2+X_9Q_3=-1$$

(A16)

where:

$$
\begin{aligned}
X_1 &= \frac{1}{qr} \\
X_2 &= \frac{A^4}{pr} \\
X_3 &= \frac{B^4}{pq} \\
X_4 &= \frac{A^2(r-p-q)}{pqr} \\
X_5 &= \frac{B^2(q-p-r)}{pqr} \\
X_6 &= \frac{A^2B^2(p-q-r)}{pqr} \\
X_7 &= \frac{p-q-r}{qr} \\
X_8 &= A^2\frac{q-p-r}{pr} \\
X_9 &= B^2\frac{r-p-q}{pq}
\end{aligned}
\tag{A17}
$$

Measuring 9 or more loads and solving (A16) using least squares approach will yield the nine values of X_1, which characterize the six-port reflectometer. With these equations one can find the characteristics which will allow us to find a unique vector.

$$
\begin{aligned}
r &= \frac{2X_5 - X_7X_9}{2X_1X_9 - X_5X_7} \\
q &= \frac{2X_4 - X_7X_8}{2X_1X_8 - X_4X_7} \\
p &= r + q + \frac{X_7}{X_1}
\end{aligned}
\qquad
\begin{aligned}
A^2 &= \sqrt{prX_2} \\
B^2 &= \sqrt{pqX_3}
\end{aligned}
\tag{A18}
$$

All values listed in equation (A18) are positive by definition. Having the values in (A18) allows (A11) to be solved for a given set of power measurements. From (A11) we get α, β and γ and from equation (A12):

$$u = \beta; v = \pm \frac{\alpha\beta + \gamma}{\sqrt{1-\alpha^2}} \tag{A19}$$

The sign ambiguity in v can be solved through the use of a single approximately known load. Thus the four-port calibration is done with 3 known and one approximately known load. The loads used for six- to four-port reduction are shown below.

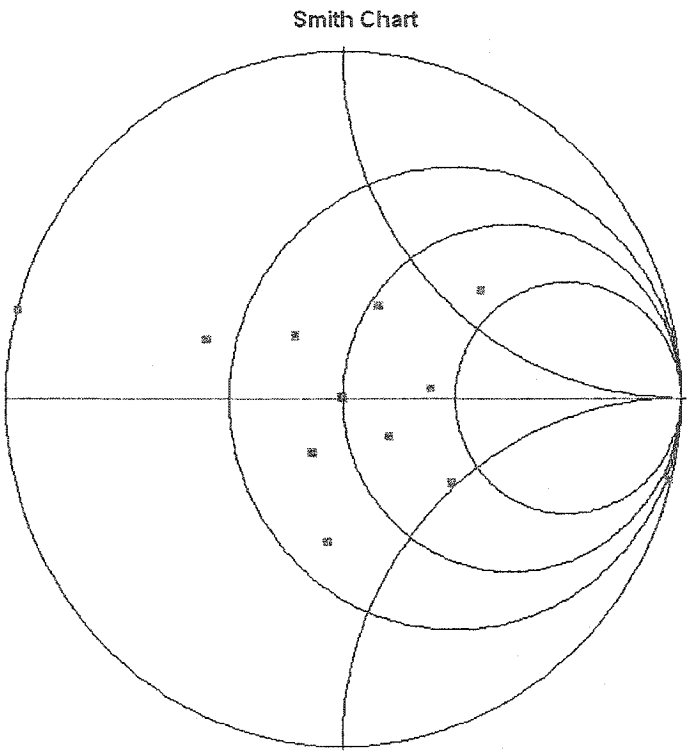

Appendix B. AMN and TRL Kit Layout

The entire circuit board and including TRL kit are shown below.

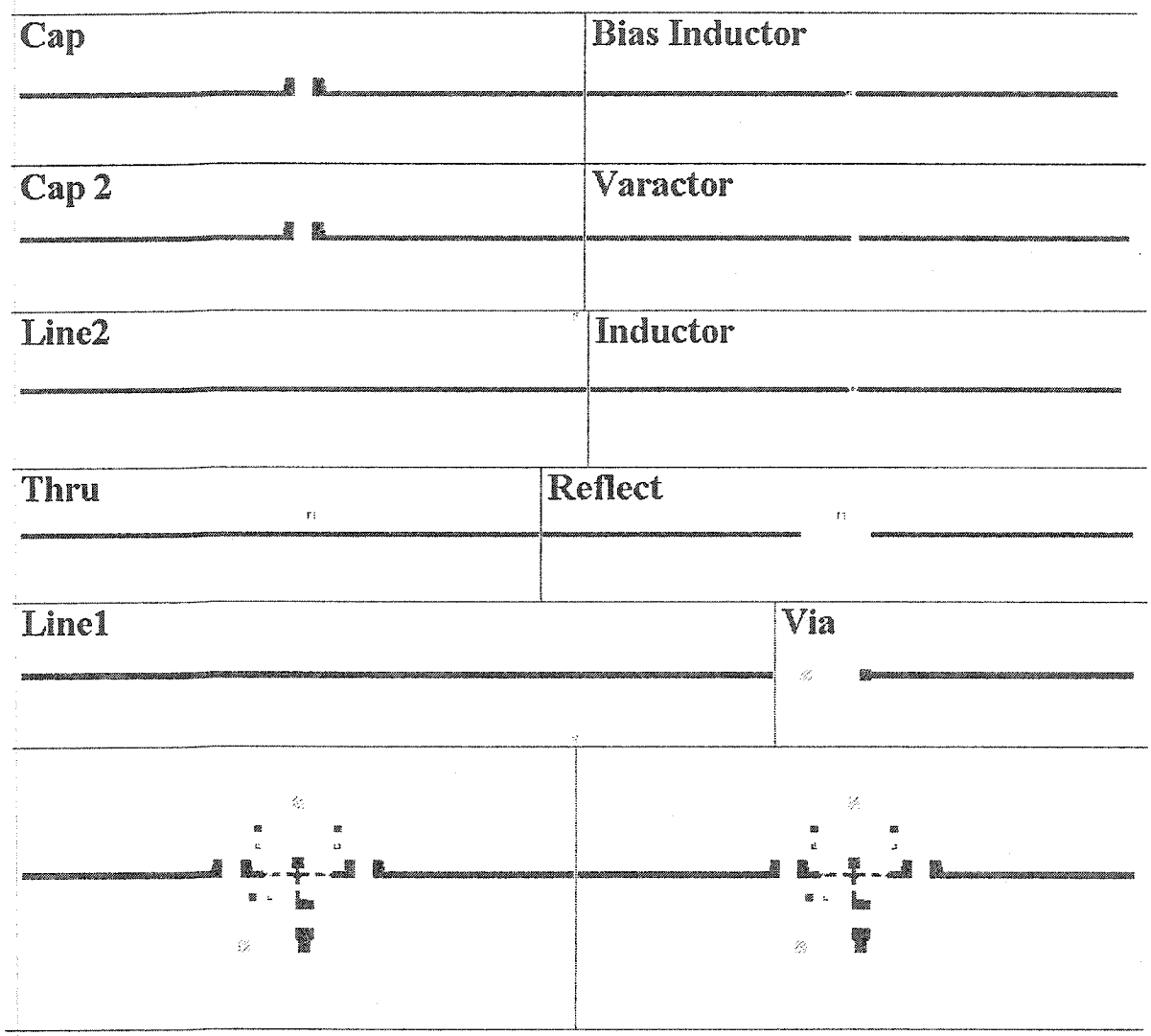

Appendix C. Simulated and Measured Components

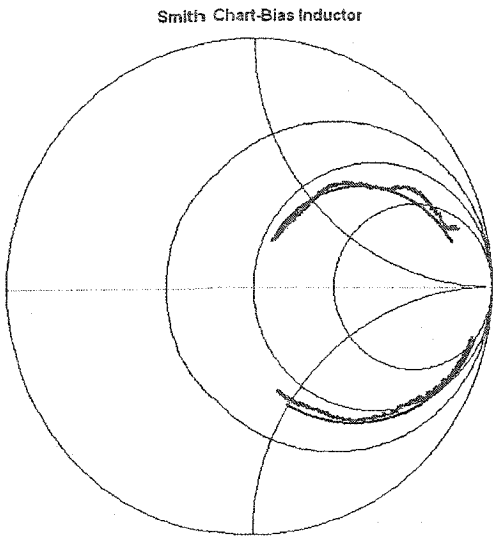

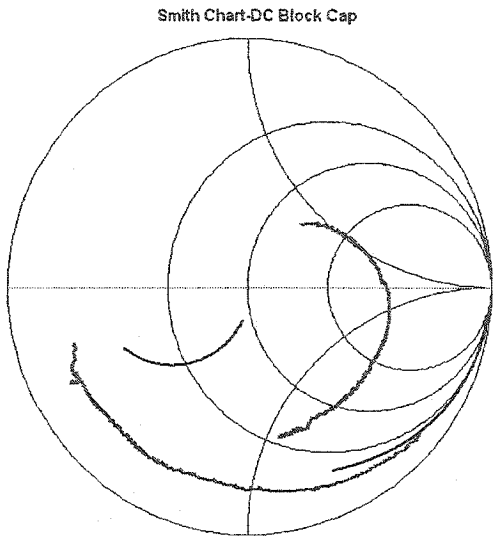

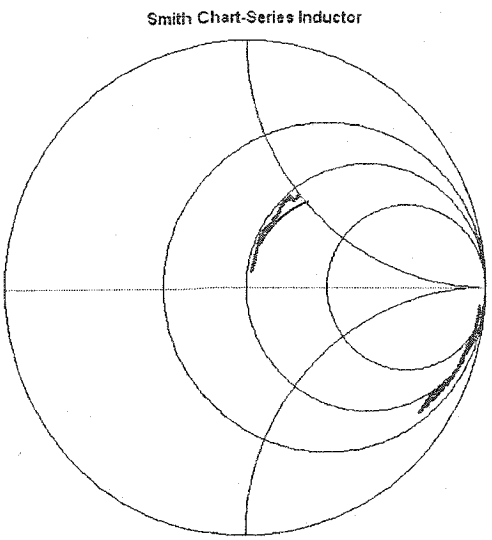

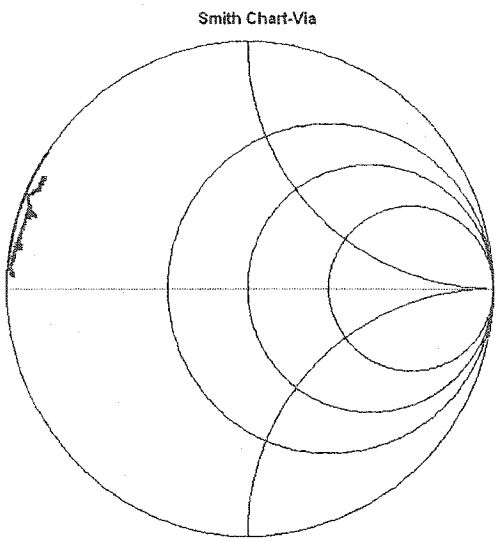

Varactor diode manufacturers Capacitance vs. Voltage.

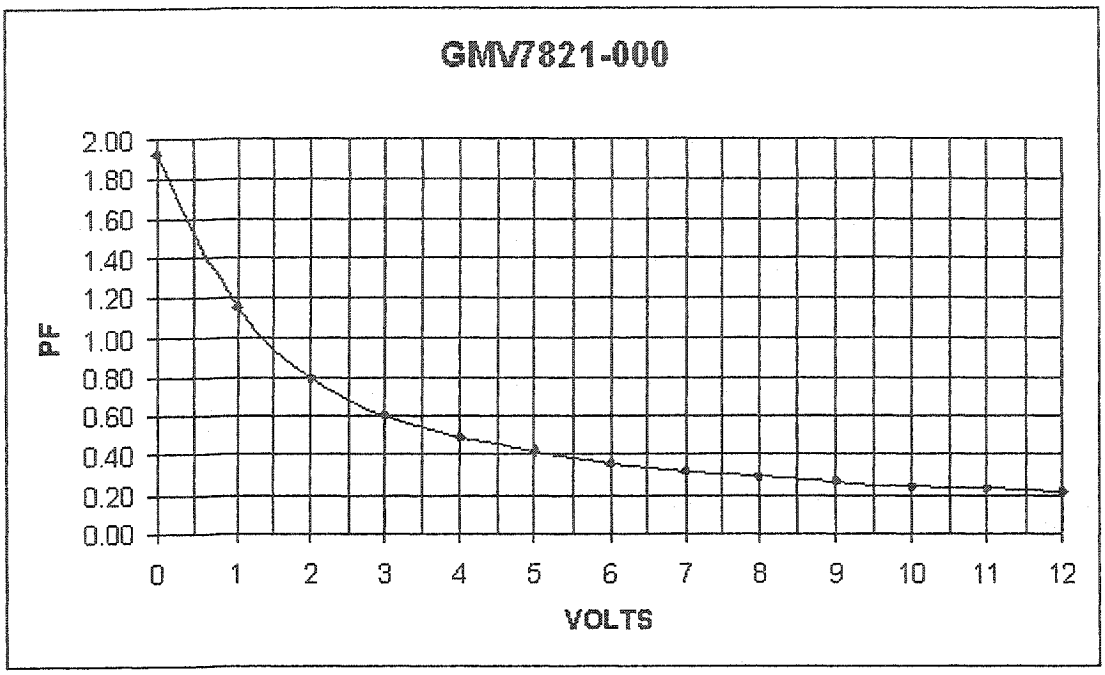

Varactor Diode Loss as a Function of Capacitance

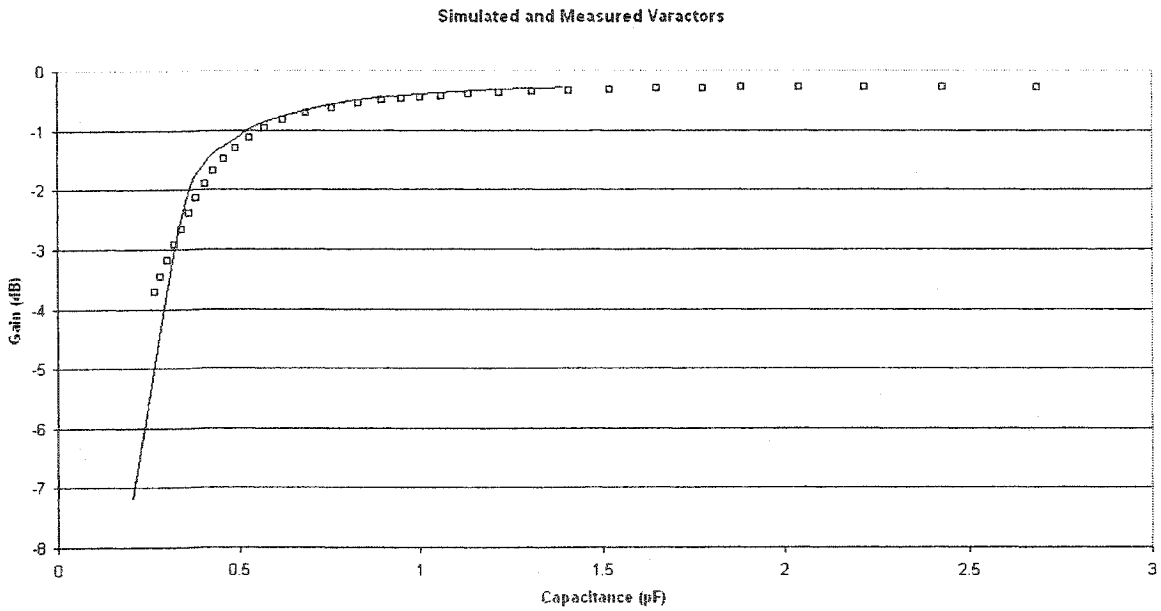

Appendix D. G_P Measurement and Matching Data

Voltage: 6 V	Current: 60 mA	
Desired gp	gp Attained	Ave % Error
1.452	1.415	2.59
1.154	1.148	0.56
0.916	0.909	1.01
0.728	0.735	1.39
0.578	0.626	8.33

Voltage: 8 V	Current: 60 mA	
Desired gp	gp Attained	Ave % Error
1.582	1.527	3.49
1.256	1.235	1.70
0.998	0.983	1.49
0.793	0.818	3.19
0.630	0.640	4.77

Voltage: 6 V	Current: 70 mA	
Desired gp	gp Attained	Ave % Error
1.472	1.416	3.79
1.169	1.160	0.78
0.928	0.925	0.79
0.738	0.762	3.30
0.586	0.608	3.86

Voltage: 8 V	Current: 70 mA	
Desired gp	gp Attained	Ave % Error
1.565	1.510	3.46
1.243	1.232	0.87
0.987	0.974	1.48
0.784	0.815	3.92
0.623	0.657	5.49

Voltage: 6 V	Current: 80 mA	
Desired gp	gp Attained	Ave % Error
1.565	1.514	3.23
1.243	1.228	1.31
0.987	0.998	1.06
0.784	0.778	0.81
0.623	0.625	1.11

Voltage: 8 V	Current: 80 mA	
Desired gp	gp Attained	Ave % Error
1.599	1.527	4.54
1.270	1.256	1.14
1.009	1.005	0.55
0.802	0.817	2.03
0.637	0.644	1.39

Voltage: 6 V	Current: 90 mA	
Desired gp	gp Attained	Ave % Error
1.454	1.424	2.10
1.155	1.149	0.63
0.918	0.912	0.75
0.729	0.724	1.62
0.579	0.648	11.87

Voltage: 8 V	Current: 90 mA	
Desired gp	gp Attained	Ave % Error
1.633	1.548	5.21
1.297	1.302	0.40
1.030	1.035	0.55
0.818	0.830	1.40
0.650	0.666	4.79

Voltage: 6 V	Current: 100 mA	
Desired gp	gp Attained	Ave % Error
1.478	1.462	1.10
1.174	1.163	0.96
0.932	0.930	1.64
0.741	0.765	3.31
0.588	0.680	15.62

Voltage: 8 V	Current: 100 mA	
Desired gp	gp Attained	Ave % Error
1.607	1.553	3.37
1.276	1.274	0.36
1.014	1.013	0.79
0.805	0.846	5.03
0.640	0.698	9.17

Voltage: 6 V	Current: 110 mA	
Desired gp	gp Attained	Ave % Error
1.522	1.512	0.68
1.209	1.202	0.60
0.960	0.966	1.72
0.763	0.796	4.30

Voltage: 8 V	Current: 110 mA	
Desired gp	gp Attained	Ave % Error
1.718	1.649	4.02
1.365	1.341	1.71
1.084	1.068	1.45
0.861	0.871	1.42
0.684	0.693	3.79

Voltage: 6 V	Current: 120 mA	
Desired gp	gp Attained	Ave % Error
1.557	1.551	0.44
1.237	1.244	0.59
0.983	1.012	3.01
0.781	0.815	4.48
0.620	0.755	21.82

Voltage: 8 V	Current: 120 mA	
Desired gp	gp Attained	Ave % Error
1.682	1.613	4.10
1.336	1.337	0.64
1.061	1.045	1.55
0.843	0.883	4.84
0.669	0.713	6.51

Appendix E. Equipment and Parts List

Equipment List
HP8510B Vector Network Analyzer
HP8340B Power Source
Anritsu ML2438A Power Meter
Anritsu ML2473A Power Sensors
Wiltron Universal Test Fixture
Wiltron K250 Bias Tees

Six-Port Parts List
Sage C218-10 10dB Couplers
M/A COM PN2089-6208-00 Power Divider
M/A COM PN2032-6371-00 Quadrature Hybrids
DMT M4-413E38T Single-Pole Four-Throw Switch

Bibliography

1. Constantine A. Balanis, *Antenna Theory; Analysis and Design.* John Wiley & Sons, 1996.
2. David M. Pozar, *Microwave Engineering*, John Wiley and Sons, 1997.
3. Steve C. Cripps, *RF Power Amplifiers for Wireless Communications.* Artech Publishing House, 1999.
4. W. Simburger, A. Heinz, H.-D. Wohlmuth, J. Bock, K. Aufinger and M. Rest, "A Monolithic 2.5V, 1W Silicon Bipolar Power Amplifier With 55% PAE at 1.9GHz," in *IEEE MTT-S Int. Microwave Symp. Dig.*, 2000, pp 853-856.
5. V. T. S. Vintola, M. Matilainen, S. J. K. Kalajo and E. A. Jarvinen, "Variable-Gain Power Amplifier for Mobile WCDMA Applications," in *IEEE Trans. Microwave Theory Tech.*, vol. 49, pp 2464-2471, Dec. 2001.
6. S. Jung, K. Kang, J.-H. Park, K.-W. Chung, Y.-K. Kim, and Y. Kwon, "Micromachined Frequency-Variable Impedance Tuners Using Resonant Unit Cells," in *IEEE MTT-S Int. Microwave Symp. Dig.*, 2001, pp 333-336.
7. M.Vai and S.Prasad, "Automatic Impedance Matching with a Neural Network," in *IEEE Microwave Guided Wave Lett.*, vol. 3 pp. 353-354, Oct. 1993.
8. D.M. Drury, D.C. Zimmerman and D.E. Zimmerman, "A Dual-Gate FET Constant Phase Power Amplifier," in *IEEE MTT-S Int. Microwave Symp. Dig.*, 1985, pp. 219-222.
9. K.H. Snow, J.J. Komiak and D.A. Bates, "Segmented and Dual-Gate MESFET's for Variable Gain Power Amplifiers in GaAs MMIC," *IEEE Trans. Microwave Theory Tech.*, vol. 36, pp. 1976-1985, Dec. 1988.
10. R.B. Culbertson and D.C. Zimmermann, "A 3-Watt X-Band Monolithic Variable Gain Amplifier," in *IEEE MTT-S Int. Microwave Symp. Dig.*, 1988 pp. 171-174.
11. B.D. Geller, F.T. Assal, R.K. Gupta and P.K. Cline, "A Technique for the Maintenance of FET Power Amplifier Efficiency Under Backoff," in *IEEE MTT-S Int. Microwave Symp Dig.*, 1989 pp. 949-952.
12. T.H. Miers and V.A. Hirsch, "A Thorough Investigation of Dynamic Bias on Linear GaAs FET Power Amplifier Performance," in *IEEE MTT-S Int. Microwave Symp Dig.*, 1992 pp. 537-540.

13. A. Platzker and S. Bouthillette, "A Variable Output, High Efficiency-Low Distortion S-Band Power Amplifiers and Their Performances Under Single Tone and Noise Power Excitations," in *IEEE MTT-S Int. Microwave Symp Dig.*, 1995 pp. 441-444.

14. A. Platzker and S. Bouthillette, "High Efficiency L-Band Variable Output Power Amplifiers for Use in Communication Systems," in *IEEE MTT-S Int. Microwave Symp Dig.*, 1993 pp. 563-566.

15. T.A. Bos and U. Lott, "PCS Amplifier with Integrated Power Control," in *IEEE MTT-S Int. Microwave Symp Dig.*, 1996 pp. 771-774.

16. T. E. Hodgetts and E. J. Griffin, "A Unified Treatment of the Theory of Six-Port Reflectometer Calibration Using the Minimum of Standards," *Royal Signals and Radar Establishment*, Report No. 83003, UK, 1983.

17. C.A. Hoer, "A network Analyzer Incorporating Six-port Reflectometers," *IEEE Trans. Microwave Theory Tech.*, vol. 25, pp. 1070-1074, Dec. 1977.

18. G.F. Engen, "The Six-port Reflectometer: An Alternative Network Analyzer," *IEEE Trans. Microwave Theory Tech.*, vol. 25, pp. 1075-1080, Dec. 1977.

19. G.F. Engen, "An Improved Circuit for Implementing the Six-port Technique of Microwave Measurements," *IEEE Trans. Microwave Theory Tech.*, vol. 25, pp. 1080-1083, Dec. 1977.

20. M.P. Weidman, "A Semiautomated Six Port for Measuring Millimeter Wave Power and Complex Reflection Coefficient," *IEEE Trans. Microwave Theory Tech.*, vol. 25, pp. 1083-1085, Dec. 1977.

21. H.M. Cronson and L. Susman, "A Dual Six-Port Automatic Network Analyzer," *IEEE Trans. Microwave Theory Tech.*, vol. 29, pp. 372-378, Apr. 1981.

22. G.F. Engen, "Calibrating the Six-port Reflectometer by Means of Sliding Terminations," *IEEE Trans. Microwave Theory Tech.*, vol. 26, pp. 951-957, Dec. 1978.

23. C.A. Hoer, "Performance of a Dual Six-port Automatic Network Analyzer," *IEEE Trans. Microwave Theory Tech.*, vol. 27, pp. 993-998, Dec. 1979.

24. G.F. Engen and C.A. Hoer, "Thru-Reflect-Line: An improved Technique for Calibrating the Dual Six-port Automatic Network Analyzer," *IEEE Trans. Microwave Theory Tech.*, vol. 27, pp. 987-993, Dec. 1979.

25. J.R. Juroshek and C.A. Hoer, "A Technique for Extending the Dynamic Range of the Dual Six-port Network Analyzer," *IEEE Trans. Microwave Theory Tech.*, vol. 33, pp. 453-459, Jun. 1985.

26. L. C. Oldfield, J.P. Ide and E.J. Griffin, "A Multistate Reflectometer," *IEEE Trans. Instrum. Meas.*, vol IM-34, pp 198-201, Jun. 1985.

27. S.P. Yeo and S.T. Jay, "Improved design for Multistate Reflectometer (with Two Power Detectrs) for Measuring Reflection Coefficients of Microwave Devices," *IEEE Trans. Instrum. Meas.*, vol 49, pp 61-65, Feb. 2000.

28. S. P. Yeo and M. Cheng, "Improved four-port instrument utilising two power detectors to measure complex reflection coefficients of microwave devices," in *IEE Electronics Letters (UK)*, 1996, vol 32, pp 565-566.